

RESEARCH ARTICLE

Control of mRNA translation by dynamic ribosome modification

Lucia Grenga^{1,2}✉, Richard Howard Little¹✉, Govind Chandra¹, Stuart Daniel Woodcock¹, Gerhard Saalbach¹, Richard James Morris³, Jacob George Malone^{1,2*}

1 Molecular Microbiology, John Innes Centre, Norwich, Norfolk, United Kingdom, **2** School of Biological Sciences, University of East Anglia, Norwich, Norfolk, United Kingdom, **3** Computational and Systems Biology, John Innes Centre, Norwich, Norfolk, United Kingdom

✉ These authors contributed equally to this work.

✉ Current address: Université Paris Saclay, CEA, INRAE, Département Médicaments et Technologies pour la Santé (DMTS), SPI, Bagnols-sur-Cèze, France

* jacob.malone@jic.ac.uk



OPEN ACCESS

Citation: Grenga L, Little RH, Chandra G, Woodcock SD, Saalbach G, Morris RJ, et al. (2020) Control of mRNA translation by dynamic ribosome modification. *PLoS Genet* 16(6): e1008837. <https://doi.org/10.1371/journal.pgen.1008837>

Editor: Lotte Søgaard-Andersen, Max Planck Institute for Terrestrial Microbiology, GERMANY

Received: May 4, 2020

Accepted: May 7, 2020

Published: June 25, 2020

Peer Review History: PLOS recognizes the benefits of transparency in the peer review process; therefore, we enable the publication of all of the content of peer review and author responses alongside final, published articles. The editorial history of this article is available here: <https://doi.org/10.1371/journal.pgen.1008837>

Copyright: © 2020 Grenga et al. This is an open access article distributed under the terms of the [Creative Commons Attribution License](https://creativecommons.org/licenses/by/4.0/), which permits unrestricted use, distribution, and reproduction in any medium, provided the original author and source are credited.

Data Availability Statement: Ribosome profiling data has been submitted to ArrayExpress, with accession number E-MTAB-5408. The mass spectrometry proteomics data have been deposited to the ProteomeXchange Consortium via the

Abstract

Control of mRNA translation is a crucial regulatory mechanism used by bacteria to respond to their environment. In the soil bacterium *Pseudomonas fluorescens*, RimK modifies the C-terminus of ribosomal protein RpsF to influence important aspects of rhizosphere colonisation through proteome remodelling. In this study, we show that RimK activity is itself under complex, multifactorial control by the co-transcribed phosphodiesterase trigger enzyme (RimA) and a polyglutamate-specific protease (RimB). Furthermore, biochemical experimentation and mathematical modelling reveal a role for the nucleotide second messenger cyclic-di-GMP in coordinating these activities. Active ribosome regulation by RimK occurs by two main routes: indirectly, through changes in the abundance of the global translational regulator Hfq and directly, with translation of surface attachment factors, amino acid transporters and key secreted molecules linked specifically to RpsF modification. Our findings show that post-translational ribosomal modification functions as a rapid-response mechanism that tunes global gene translation in response to environmental signals.

Author summary

In the soil bacterium *Pseudomonas fluorescens*, root colonisation is controlled by RimK, a glutamate ligase found in many different bacterial species. By modifying the ribosomal protein RpsF, RimK changes the translation of a range of different colonisation-related genes. This in turn enables bacteria to effectively adapt to the root environment. In this study, we first unravel the regulation of RimK by the signalling molecule cyclic-di-GMP (cdG) and the enzymes RimA and RimB. We show how interactions between cdG, the RimA phosphodiesterase, the RimB protease and the RimK ligase produce an elegant regulatory circuit that translates cdG concentration into the proportion of cellular ribosomes that are modified by RimK activity. Next we examine the consequences of this ribosomal modification for mRNA translation and bacterial behaviour. RimK activity indirectly

PRIDE partner repository with the dataset identifier PXD017233. All other data is presented in the manuscript and supporting information.

Funding: RJM, JGM, RHL, GS and GC were funded by UK Research and Innovation | Biotechnology and Biological Sciences Research Council (BBSRC) Institute Strategic Program Grants BB/J004553/1 (Biotic Interactions) and BBS/E/J/000PR9797 (Plant Health) to the John Innes Centre. LG, JGM and RHL were also funded by BBSRC Responsive Mode Grant BB/M002586/1 to JGM. SDW was funded by a BBSRC DTP PhD studentship. The funders had no role in study design, data collection and analysis, decision to publish, or preparation of the manuscript.

Competing interests: The authors have declared that no competing interests exist.

controls the abundance of the global translational regulator Hfq. This leads to the regulation of a range of root colonisation genes. Furthermore, the RimK ribosomal modification directly affects translation of a second set of genes, with secreted molecules, surface attachment factors and amino acid transporters rapidly responding to changes in ribosomal modification. Thus, RimK ribosomal modification enables bacterial gene translation to rapidly adapt to changing environmental signals in the complex root environment.

Introduction

The plant rhizosphere is a highly complex environment, comprising an intricate spatial organisation of roots and soil, with thousands of competing and cooperating microorganisms linked by dynamic fluxes of nutrients, toxins and signalling molecules [1, 2]. Microbial rhizosphere colonisation is a correspondingly complex, multi-stage process by which soil-associated bacteria spatially explore, exploit and defend the root environment [3]. The colonisation process begins with chemotaxis to the rhizosphere along an exudate gradient, followed by surface adhesion, migration across the root surface [4] and biofilm formation [5].

To enable effective rhizosphere colonisation, soil bacteria sense many different environmental inputs and translate them into an integrated phenotypic response. This requires an interconnected network of signal transduction systems functioning at multiple regulatory levels, including gene transcription [6], modulation of translational activity [7] and changes in protein function [8]. The cyclic-di-GMP (cdG) signalling network mediates the switch between motile and sessile lifestyles in many bacterial species [9] and is a key regulator of rhizosphere colonisation in multiple plant-associated microbes [10–13]. CdG signalling in *Pseudomonas* forms a highly complex, non-linear and pleiotropic network, with multiple connections to other signalling systems and phenotypic outputs that vary profoundly in response to environmental cues [14, 15]. The model *P. fluorescens* strain SBW25, for example, contains over 40 cdG-metabolic enzymes [16] that influence phenotypes at every regulatory level and whose expression varies throughout rhizosphere colonisation [11]. *Pseudomonas* cdG signalling shows extensive overlap with other global gene regulators, such as Gac/Rsm [17, 18] and the RNA-chaperone Hfq [19].

In *P. fluorescens*, Hfq is important for niche adaptation, with deletion mutants displaying strongly reduced motility, increased surface attachment, and severely compromised rhizosphere colonisation [14, 19]. The regulatory connections between cdG and Hfq are reflected in the close phenotypic parallels between mutants in both pathways [19–21].

We recently identified a further contributor to the post-transcriptional regulatory network in *Pseudomonas* spp. [19]. Similar to Hfq and cdG, the ribosomal modification protein RimK controls the transition between active and sessile bacterial lifestyles. RimK is an ATP-dependent glutamyl ligase that adds glutamate residues to the C-terminus of ribosomal protein RpsF, which in-turn induces specific changes in the bacterial proteome [19]. RimK activity is itself controlled by binding to cdG and the small proteins RimA and RimB. RimK exerts at least some of its regulatory activity indirectly through Hfq, with reduced Hfq levels observed in an SBW25 $\Delta rimK$ background [14].

Our research to date leads to a model connecting RimK glutamation of RpsF with proteomic changes that enable environmental adaptation by *Pseudomonas*. Nonetheless, at this stage several key questions remain unanswered. The Rim pathway clearly responds to environmental cues that vary during rhizosphere colonisation [19]. However, the nature of these signals and mechanisms by which they control RimK activity are currently unknown, and the

relationship between the three Rim proteins and cdG is poorly defined. How RimK modification of RpsF induces downstream effects in the *Pseudomonas* proteome is also not well understood. In particular, we do not understand the extent to which RimK activity is mediated through altered Hfq levels as opposed to other mechanisms, and whether changes in RpsF modification lead directly to altered mRNA translation.

To address these outstanding questions, we used a combination of protein biochemistry, computational modelling, quantitative proteomics and ribosomal profiling (Ribo-seq) to interrogate Rim system function and the relationship between ribosomal modification and changes in the SBW25 proteome. We show that RimK controls proteome remodelling by two distinct routes. Indirectly, the Rim system induces media-dependent changes in Hfq abundance, as described previously [19]. Independent of these Hfq-mediated effects, RpsF glutamation leads to altered translation of a subset of genes including surface attachment factors and amino-acid metabolism. Rim-induced proteomic changes occur rapidly when bacteria are exposed to Rim activating conditions, confirming that ribosomal modification by RimK functions as a previously uncharacterised, actively regulated mechanism enabling rapid proteome adaptation in response to changes in the rhizosphere environment.

Results

Expression of the *rimABK* operon is controlled by temperature and nutrient availability

Our previous analysis of the expression of the *P. fluorescens* SBW25 *rim* operon throughout rhizosphere colonisation [19] suggested that it was subject to control by uncharacterised signals from the rhizosphere environment and prompted us to investigate the *rimABK* operon in more detail. First, RT-PCR was used to show that the three *rim* genes are transcribed as a single polycistronic operon (S1A Fig), whose transcriptional start site was mapped to 28–30 bp upstream of the *rimA* ORF using 5' RACE (S1B Fig). To examine the relationship between *rim* expression and environmental signals in more detail, we used qRT-PCR to quantify *rimK* mRNA abundance in SBW25 exposed to a variety of different nutrient conditions and abiotic stresses. Significant increases in *rimK* expression were observed for cells transferred to low temperature (8°C) and exposed to nutrient-limiting conditions (Fig 1), consistent with earlier findings that *rim* expression is reduced in the established (nutrient-replete) wheat rhizosphere [19]. Relative levels of *rimA* mRNA quantified under the same growing conditions do not substantially differ from those seen for *rimK* (S1C Fig), strongly suggesting that the identified promoter controls the expression of all three *rim* genes.

RimA and cdG stimulate RimK ATPase activity and RpsF glutamation

Our initial study suggested that a major element of RimK regulation is mediated post-transcriptionally, by interaction with RimA, RimB and the second messenger molecule cdG [19]. At this stage, how the RimABK-cdG system functions to control ribosomal protein modification remains unknown. To address this, we developed kinetic models of the system and conducted a series of biochemical experiments, measuring the effects of each regulator individually and in combination on RimK activity.

The effects of both RimA and cdG on RimK ATPase activity were dependent on a roughly equimolar ratio of protein/messenger with RimK (Fig 2A–2E). Combined with earlier observations [19], this strongly suggests that RimK activity is controlled by direct interaction in each case. A simple explanation for the change in RimK activity is that RimK can exist in two conformational states, one with basal activity and one with higher activity. To evaluate this

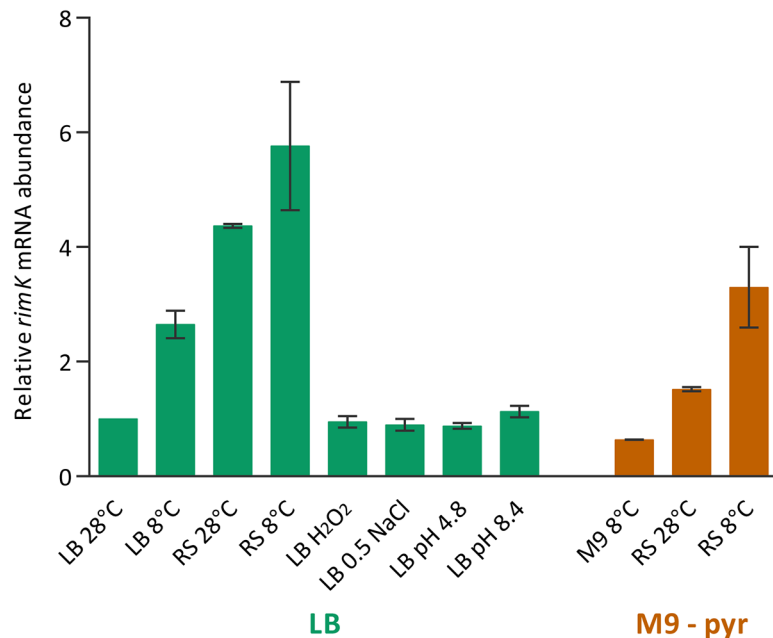


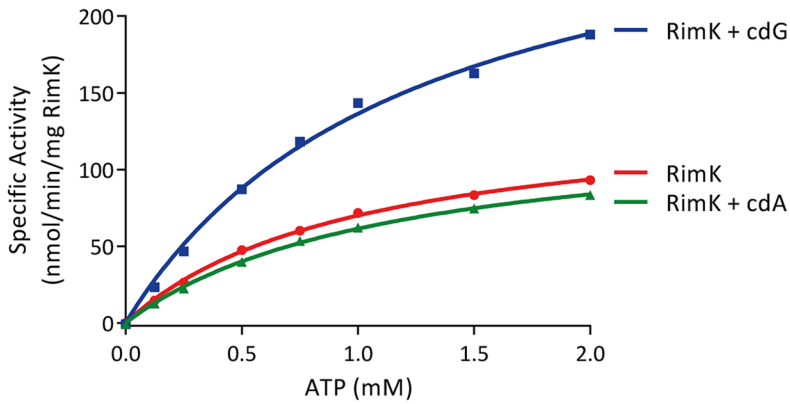
Fig 1. *rimK* expression is stimulated by low temperature and nutrient starvation. mRNA abundance (qRT-PCR data) relative to cells grown overnight in LB and transferred to LB at 28°C for 45 minutes. In each case cells were grown in LB or M9-pyruvate and transferred to a new set of conditions for 45 minutes prior to sampling. RS—carbon free ‘Rooting Solution’ [19], H₂O₂—LB containing 1.0 mM H₂O₂, LB 0.5 NaCl—LB containing 0.5 M NaCl. Data are presented +/- the standard error of three replicates. The experiment was repeated three times independently and a representative is shown.

<https://doi.org/10.1371/journal.pgen.1008837.g001>

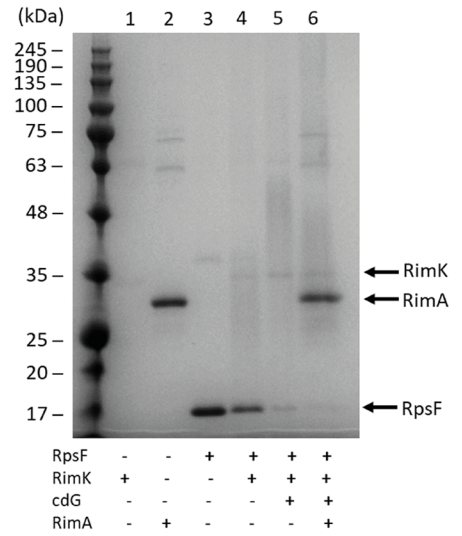
hypothesis, we built models of protein binding based on mass action kinetics for the individual reactions (S1 Table). The two-state model captures the behaviour of each of the individual experiments, however, the predicted differences in the equilibrium binding constants are not consistent with existing data (S2 Fig). Using $K_d = 1 \mu\text{M}$ for cdG binding to RimK [19] leads to 96% of RimK being in a cdG bound state under the experimental conditions and predicts a marginal ATPase activity increase upon addition of RimA for a two state model. Experimental validation qualitatively confirms this increase but quantitatively falsifies the two-state model, showing that the effects of RimA and cdG are approximately additive (Fig 2E). This suggests that RimK can exist in at least four different states with varying ATPase activities (S1 Table). This four-state model of RimK ATPase activity provides a good quantitative fit with the experimental data as well as reasonable K_d values (S2 Fig).

To determine whether RimK ATPase activity was a good proxy for RimK glutamate ligase activity on RpsF we extended our experiments to include RpsF. In agreement with our earlier work [19], cdG was shown to stimulate both ATPase activity (Fig 2A) and RpsF modification (Fig 2B), as indicated by the reduced amount of the unmodified RpsF fraction and the appearance of a smear of protein density throughout the gel (Lanes 5–6, [19]). This stimulation was highly specific, as incubation with the dinucleotide signalling molecule cyclic-di-AMP had no effect (Fig 2A). RimA addition also directly and specifically boosted RimK enzyme activity (Fig 2C and 2D). As previously demonstrated [19], the effect of RimA addition was not influenced by the presence of a, potentially inactive, cleavage product contingent on the RimA stability *in vitro*. Furthermore, this stimulation was additive with that provided by cdG (Fig 2B, Lane 6).

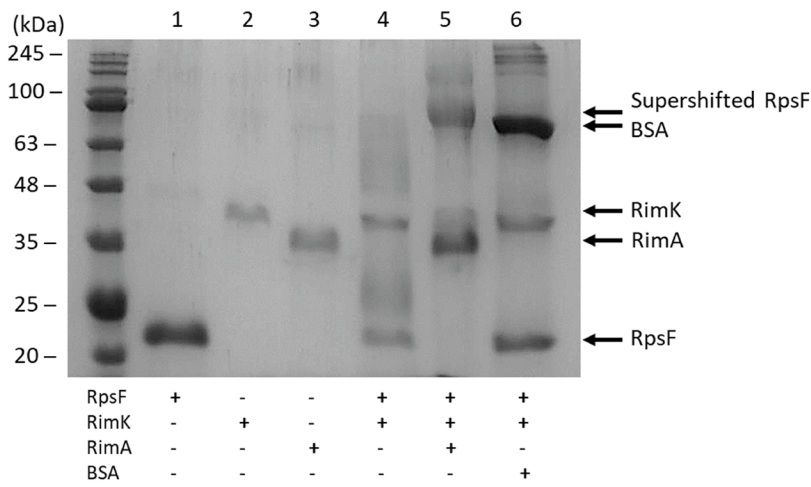
A



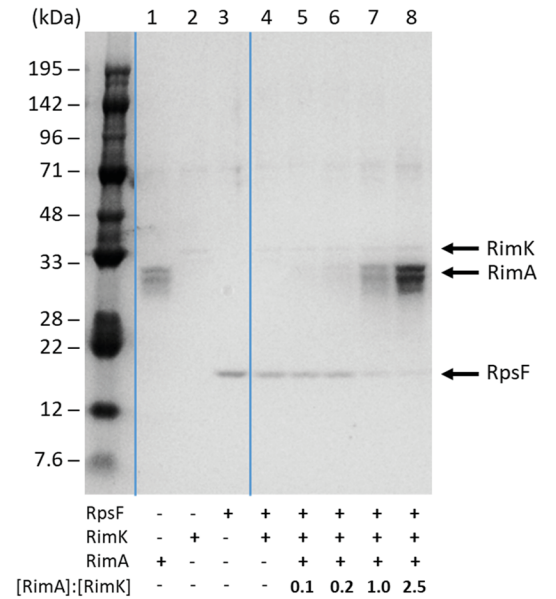
B



C



D



E

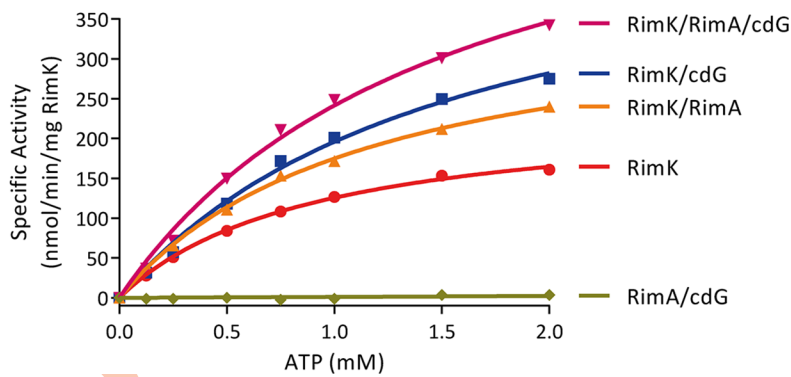


Fig 2. (A) CdG stimulates RimK ATPase activity. RimK was present at a concentration of 2.5 μM . Nucleotides were present at a concentration of 25 μM . **(B) CdG and RimA additively accelerate the rate of RpsF modification.** 12.5% SDS-PAGE gel. *E. coli* RpsF, SBW25 RimK and SBW25 RimA were present at a concentration of 6.4 μM , 3.8 μM and 3.9 μM respectively. The positions of RimK, RimA and RpsF are indicated. CdG was present at a concentration of 150 μM . The samples were incubated overnight prior to electrophoresis. Modification of RpsF by RimK is inversely related to the intensity of the indicated RpsF band. **(C) RimA alone accelerates the rate of RpsF modification.** 12.5% SDS-PAGE gel. *E. coli* RpsF was present at a concentration of 13.6 μM and SBW25 RimK and RimA were present at a concentration of 3.8 μM and 3.9 μM respectively. The position of a super-shifted RpsF band in the penultimate lane and the positions of RimK, RimA, RpsF and BSA are also indicated. The samples were incubated overnight prior to electrophoresis. **(D) Equivalent concentrations of RimA are required to stimulate RimK modification activity.** Samples were run on a 12.5% SDS-PAGE gel. *E. coli* RpsF was present at a concentration of 6.8 μM , SBW25 RimK at 1.9 μM . RimA was present at the indicated ratio relative to RimK in each case. The positions of RimK, RimA and RpsF are indicated. Samples were incubated for 60 minutes prior to electrophoresis. **(E) The ATPase activity of RimK is stimulated additively by RimA and cdG.** SBW25 proteins were present at 1 μM . CdG was present at a concentration of 25 μM .

<https://doi.org/10.1371/journal.pgen.1008837.g002>

RimB stimulates RimK ATPase activity, but suppresses RpsF glutamation

To investigate the effect of RimB, we incubated RimK with RimB and observed a marked increase in RimK ATPase activity, beyond that achieved by addition of RimA and cdG (Fig 3A, [19]). This ATPase activity could not be captured by the previous four state model of RimK, leading us to hypothesise a further level of activation (S1 Table). Based on our experiments with RimA and cdG, we predicted that increased ATPase activity would translate to enhanced glutamate ligase activity. Interestingly however, this was not the case. Not only was the observed ATPase activity increase largely abolished by addition of RpsF to the reaction (Fig 3A), RimB addition produced a strong suppressive effect on the ability of RimK to shift the RpsF band in our glutamation assays (Fig 3B, [22]). A possible explanation is that RimB blocks access of RimK to RpsF. To test this hypothesis, we measured the effect of different concentrations of RimB. The prediction is that comparable amounts of RimB would be required to largely saturate RimK and render it inactive for RpsF glutamation. We found that the suppressive effect was indeed strongly dependent on the concentration of RimB in the reaction (Fig 3C) but that surprisingly small concentrations of RimB were sufficient to reduce glutamation, arguing against a stoichiometric binding model of RimK inhibition. This decrease could only be partially countered by increasing glutamate concentration (Fig 3C), eliminating glutamate availability as the cause of RimB suppression of RpsF band-shifting under our test conditions. Thus, RimA, RimB and cdG enhance RimK ATPase activity, and RimA and cdG enhance but RimB suppresses RimK glutamylation activity.

Interestingly, RimA was able to boost the RpsF modification activity of RimK even in the presence of RimB (Fig 3D, Lanes 8–9). Based on our RimK ATPase data we would expect cdG to boost RpsF modification even further. Puzzlingly, increasing concentrations of cdG actually attenuated the effect of RimA, evidenced by an increasing concentration of smaller molecular weight glutamated RpsF species (Lanes 10–13). This effect appeared to be dependent on the presence of RimB as no attenuation of RimA stimulation of RimK modification activity was observed in the absence of RimB (Lanes 6 and 7). The suppressive effect of cdG on RimK behaviour was dependent on the phosphodiesterase activity of RimA. An enzymatically inactive RimA variant (RimA-E47A) was able to stimulate RimK activity both in the presence or absence of cdG despite being less tractable to purification than the wild-type protein (Fig 3E).

Despite RimB and RimK being co-expressed (S1A Fig) and interacting directly with one another [19], the strong RimB suppression of RimK band-shifting still occurred when the ratio between RimB and RimK was as low as 1:63 (Fig 3C). This strongly argues against a mechanism for RimK regulation based on direct interaction with RimB. This falsifies our initial model in which we suggested that RimB functions as a direct regulator of RimK activity [19] and together with the suppression effect of cdG highlights complexities not accounted for in our stoichiometric kinetic model.

dependent manner. 12.5% SDS-PAGE gel. *E. coli* RpsF, SBW25 RimK, SBW25 RimA and SBW25 RimB were present at a concentration of 6.8 μM , 3.8 μM , 3.9 μM and 6.0 μM respectively. The blue triangle represents increasing cdG concentrations of 5, 10, 50 and 200 μM . Lanes 9 and 11 (containing WT RimA) show increasing densities of low molecular weight RpsF species upon addition of cdG. The positions of RimK, RimA and RpsF (prior to modification) are indicated. **(E) A CdG binding mutant of RimA is able to fully stimulate RimK modification activity in the presence of the nucleotide.** 12.5% SDS-PAGE gel. *E. coli* RpsF, SBW25 RimK and SBW25 RimA proteins were present at a concentration of 6.8 μM (due to the intractable nature of the protein to purification and the contribution of contaminants to protein quantitation assays, the intensity of the RimA-E47A band is weaker than the RimA wild-type band), 3.8 μM and 3.9 μM respectively where indicated. RimB was present at either 1.7 μM (denoted by a single cross below the gel) or 3.4 μM (denoted by a double cross below the gel). Cyclic-di-GMP is present at a concentration of 200 μM . Lanes 14 and 16 (containing RimA-E47A) reveal loss of the unmodified RpsF band and increasing intensity of larger species upon cdG addition. The positions of RimK, RimA and RpsF (prior to modification) are indicated.

<https://doi.org/10.1371/journal.pgen.1008837.g003>

RimB functions as a specific protease for the modified C-terminal of RpsF

The above observations suggest an enzymatic role for RimB. RimB shows modest secondary structural similarity to Pfam class PF05618 (ATP-dependent zinc proteases), leading us to hypothesize that the apparent suppression of RpsF band-shifting may represent cleavage of C-terminal poly-glutamate (poly-E) tails, following their addition by RimK. This would potentially explain how relatively low amounts of RimB are able to effectively prevent RpsF band-shifting by RimK. To test this, we first examined the effect of adding purified RimB to RpsF samples that had been previously glutamated by RimK addition (Fig 4A). Addition of RimB to RimK-modified samples restored the RpsF bands to their original gel positions, consistent with cleavage of the poly-E tail. To exclude the possibility that RimB activity may be mediated through RimK, we purified and incubated with RimB a modified RpsF allele (RpsF_{10glu}) with 10 additional C-terminal glutamate residues. The RimB protein was able to reduce the mass of RpsF_{10glu} towards that of WT RpsF, confirming its protease activity (Fig 4B). No effect was seen on RimB incubation with unmodified RpsF, suggesting that RimB acts to remove poly-E tails specifically rather than as a protease for the unmodified RpsF protein.

Mass spectrometry analysis of the RpsF bands from the experiment in Fig 4A indicated that RimB protease activity in fact left 4–5 glutamate residues at the RpsF C-terminus. To investigate this activity further, different combinations of RimK, RimA and glutamate were combined *in vitro* and incubated for 60 minutes prior to separation by SDS-PAGE and mass spectrometry analysis to determine the RpsF glutamation state (Fig 4C). As predicted, addition of RimK resulted in unregulated modification of RpsF_{10glu} in a glutamate-dependent manner (Lanes 4–6). Introduction of RimB to RpsF_{10glu} at a concentration of 6 μM resulted in the removal of C-terminal glutamates from RpsF irrespective of the presence of glutamate (Lanes 8 and 9). In the presence of RpsF_{10glu} and RimK, increasing concentrations of RimB partially restored protein density in the RpsF region of the gel (Lanes 10 and 11). Removal of glutamate residues from RpsF by RimB was augmented in the absence of externally added glutamate, presumably due to reduced RimK glutamation activity (Lane 12). In the presence of RpsF_{10glu}, 60nM RimB, glutamate and elevated levels of RimK, no RpsF protein was detected in the RpsF region of the gel due to hyper-modification by RimK ([19], Lane 13). Increasing [RimB] to 6 μM restored protein density to the RpsF region of the gel, although glutamate chain lengths of up to 13 residues were still obtained (Lane 14). Removal of glutamate under these conditions reduced the extent of glutamation, but not to the extent of Lanes 8 and 9, indicating that RimK is able to utilise glutamate liberated from RpsF_{10glu} by RimB (Lane 15).

Computational models postulate that addition and proteolytic removal of glutamates can lead to systemic addition of ~4 glutamates to many ribosomes

To explain the complex interplay observed in this system, we incorporated protease activity of RimB into a model for RpsF glutamation. We built a stochastic model for chain extension,

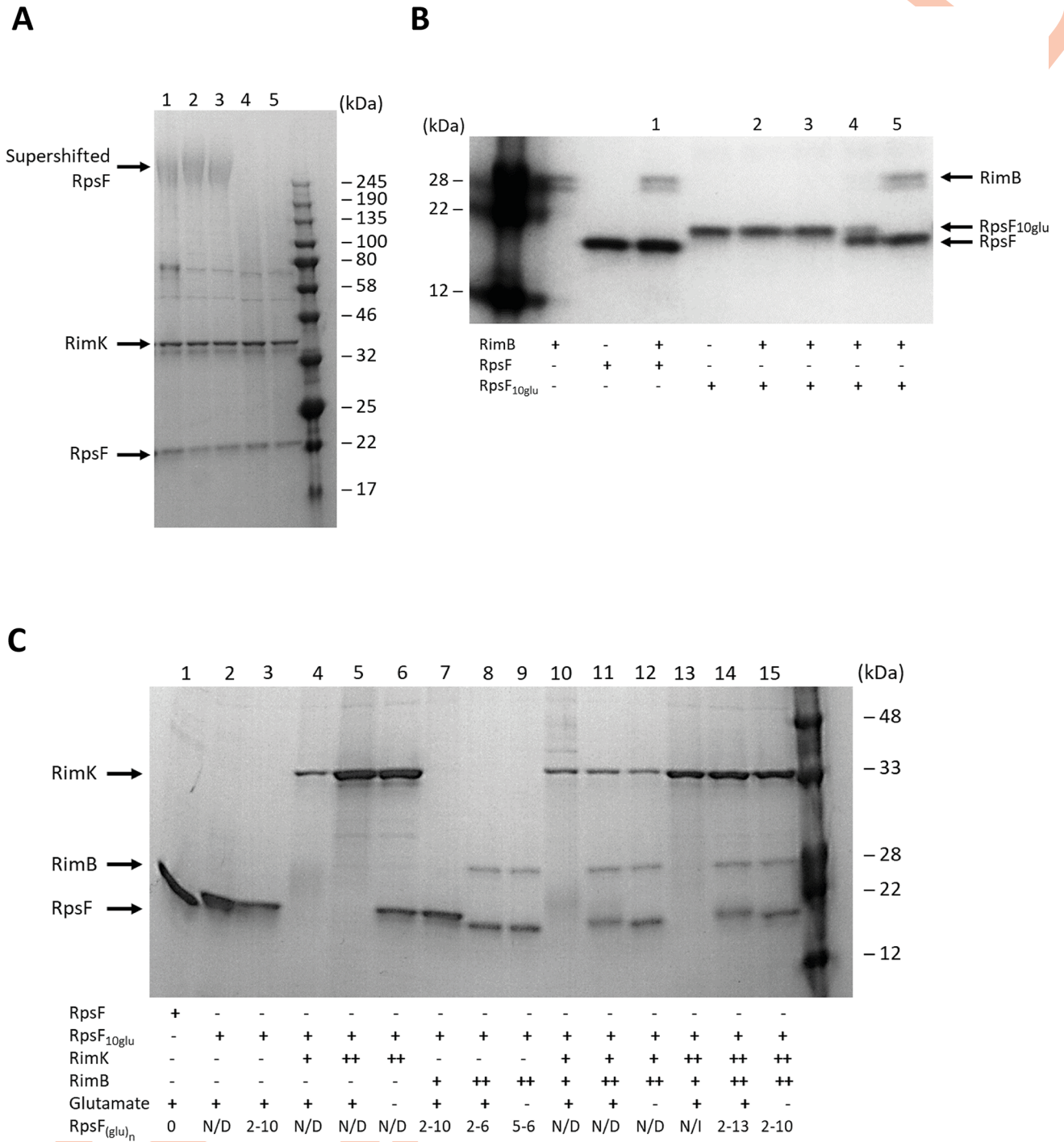


Fig 4. (A) The presence of RimB abolishes the poly-glutamated form of RpsF. 12.5% SDS-PAGE gel. SBW25 RpsF was present at a concentration of 12.8 μM. SBW25 RimK was present at a concentration of 15 μM. Samples were incubated overnight to allow formation of the modified RpsF species shown in Lane 1. The sample was divided into four equal volumes and the following additions made: Lane 2 –buffer only; Lane 3 – 20mM ADP; Lane 4–100 nM SBW25 RimB; Lane 5–100 nM SBW25 RimB + 20 mM ADP. After 150 minutes incubation, samples were taken for SDS-PAGE analysis. The positions of the supershifted RpsF band, RimK and unmodified RpsF (Lane 1) are indicated. **(B) RimB proteolyzes poly-glutamated RpsF.** 12.5% SDS-PAGE gel. SBW25 RpsF and RpsF_{10glu} were present at a concentration of 12.8 μM. RimB concentrations in the lanes labelled 1–5 were: Lane 1–6.0 μM; Lane 2–6.0 nM; Lane 3–60 nM; Lane 4–600 nM; Lane 5–6.0 μM. After 5 minutes incubation, samples were withdrawn for SDS-PAGE analysis. The positions of RimB, unmodified RpsF and RpsF_{10glu} are indicated. **(C) RimB cleaves glutamate residues from the C-terminus of RpsF.** 12.5% SDS-PAGE gel. SBW25 RpsF and RpsF_{10glu} were present at a concentration of 12.8 μM. SBW25 RimK was present at a concentration of either 3.8 μM (denoted below the gel as a single cross) or 15 μM (a double cross). SBW25 RimB was present at a concentration of either 60 nM (denoted below the gel

as a single cross) or 6.0 μM (a double cross). After 60 minutes incubation, samples were withdrawn for SDS-PAGE analysis. Following SDS-PAGE, gel slices were excised from the region of the gel defined by the unmodified and partially modified RpsF bands present at the base of the gel and submitted for mass spectrometric analysis. N/D = Not Determined; N/I = Nil Identified. The positions of RimK, RimA and RpsF are indicated.

<https://doi.org/10.1371/journal.pgen.1008837.g004>

assuming that without RimB, chain extension is processive and RimK can either add a glutamate or release RpsF. Depending on RimK activity, this can lead to very long glutamate chains. Within the model we set a chain length limit of 100 glutamate units (Fig 5A). We then included the action of RimB, cutting the chains from the end, one unit of glutamate at a time, down to the experimentally determined resultant minimal length of four. Unsurprisingly, this results in seemingly futile cycles of RpsF glutamation by RimK followed by cleavage by RimB. The balance between RimK glutamate ligase activity and RimB protease activity determines the dynamics of RpsF glutamate chain lengths and average chain length distribution (Fig 5A).

To more realistically model the *in vivo* relationship between the Rim system and the highly abundant RpsF protein, we estimated that a typical cell contains approximately 1 RimABK complex to every 500 RpsF units. This means that in order to understand the overall impact of RimB on the system, we need to consider how the population of RpsF behaves as a function of cdG (i.e. variable RimK activity, assuming RimB activity is constant). Fig 5B shows the distribution of glutamate chain lengths for a population of RpsF molecules. In the absence of RimB, the chain length distribution is broad and importantly we can expect a large number of RpsF proteins to have no glutamate chains at all. With active RimB present, a limited glutamate pool can be effectively equally distributed over all RpsF units in the cell, thus enabling a uniform switch of RpsF. These simulations suggest the striking results of a changing RimB protease activity vs RimK glutamate ligase activity (governed by cdG) on the number of RpsF units that can be modified. If this global coverage is important, this points to chain lengths of 4 being sufficient to give rise to a change in translation that would allow for a rapid and coordinated response to environmental cues.

Our *in vitro* data (Fig 4) suggests that RimB proteolytic activity alone cannot restore RpsF to the unmodified state. Thus, to satisfy our model for dynamic ribosomal modification by RimK it is necessary to invoke the presence of a second, 'reset' protease that removes post-translational glutamates from RpsF. To seek evidence for additional proteolysis of RpsF, we constructed SBW25 strains in which the *rpsF* gene was extended by 10 glutamate residues. Samples were then grown to exponential or stationary phase and probed with antibodies against RpsF and poly-glutamate (Fig 6). Cells expressing RpsF_{10glu} from an otherwise WT background revealed significant degradation of the RpsF C-terminal tail in comparison to RpsF protein levels under stationary phase conditions where ribosome neogenesis will be severely limited. The loss of the C-terminal poly-glutamate tail was even more pronounced in a $\Delta rimK$ background. Crucially, cells lacking *rimB* also showed strong reduction of RpsF glutamate tails relative to RpsF levels under stationary phase conditions, consistent with a second, RimB-independent mechanism for RpsF C-terminal degradation.

Environmental inputs rapidly affect protein abundance in a RimK dependent manner

To test whether RimK modification of RpsF represents a rapid, active cellular response to environmental signals, we examined the short-term impact of RimK stimulation on the bacterial proteome. Our qRT-PCR data (Fig 1) indicates that *rim* mRNA abundance is promoted in cold, starved cells. Therefore, overnight cultures of WT SBW25 and $\Delta rimK$ cells grown at 28°C in LB media were abruptly transferred to 8°C in nutrient-limiting rooting solution (A), and 28°C in LB media (B) for 45 minutes. We then conducted a quantitative proteomic analysis

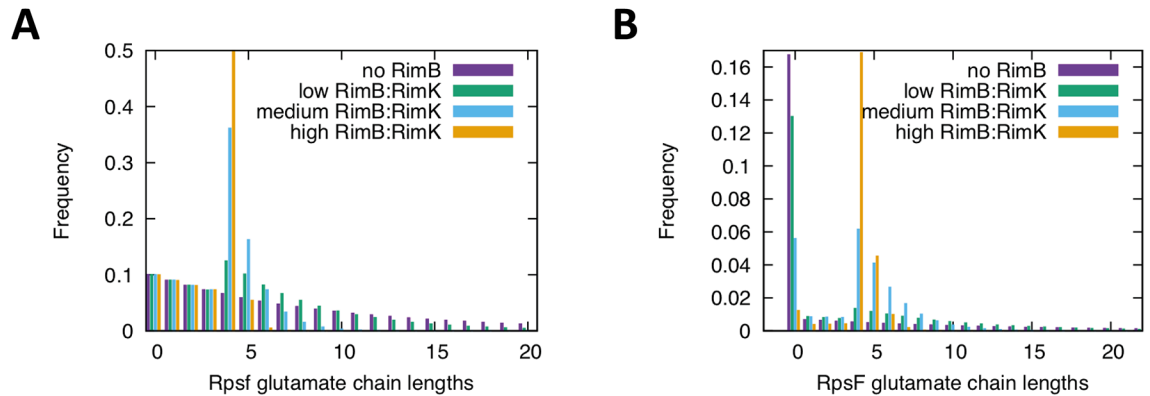


Fig 5. (A) Changing the ratio of protease activity of RimB to RimK glutamate ligase activity changes the glutamate chain length distribution of RpsF. Stochastic simulations of glutamate addition, chain termination and chain cleavage were average over 1,000,000 simulations to obtain the expected chain length distributions as a function of a changing RimB:RimK activity ratio. As has been previously shown, with no dependency of the chain extension and termination probabilities, the chains follow an exponential distribution (purple curve, no RimB protease activity). Introducing RimB protease activity results in longer chains being reduced in length and shifting the distribution towards to minimal length at which RimB is active (four units). Increasing RimB:RimK activity further pushes the chain length distribution to peak sharply around a length of four. By changing the activity of RimK, RimA and cdG can change the ratio of protease to glutamate ligase activity in the system, with an increasing ratio sharpening the chain length distribution around four. **(B) High levels of cyclic di-GMP increase the ratio of RimB protease activity to RimK glutamate ligase activity,** leading to a shift towards shorter glutamate chains on RpsF and wider coverage of RpsF modification. For a limited amount of glutamate in the system and the high RpsF to RimABK ratio, the average chain lengths (Fig 5A) can lead to drastic changes in the overall modification of ribosomal units. With reduced RimB protease activity vs RimK glutamate ligase activity, a few long chains are produced on some RpsF but the majority have no chains at all (purple, no RimB protease activity). With a higher ratio of RimB protease activity vs RimK glutamate ligase activity, RimK delivers high coverage of shorter chains to more RpsF units (green to blue to orange). This protease to glutamate ligase activity is regulated by cdG and [glutamate]. Stochastic simulations were averaged from 1,000,000 runs using 500 RpsF to every RimABK.

<https://doi.org/10.1371/journal.pgen.1008837.g005>

experiment using isobaric labelling (iTRAQ) to examine how these conditions affected protein abundance in the WT and mutant backgrounds. When a 2D scatter plot was constructed for this data (Fig 7), proteins whose conditional abundance changes are unrelated to *rimK* deletion sit along a line with gradient +1 ($x = y$). Deviation from the $x = y$ line indicates an effect of

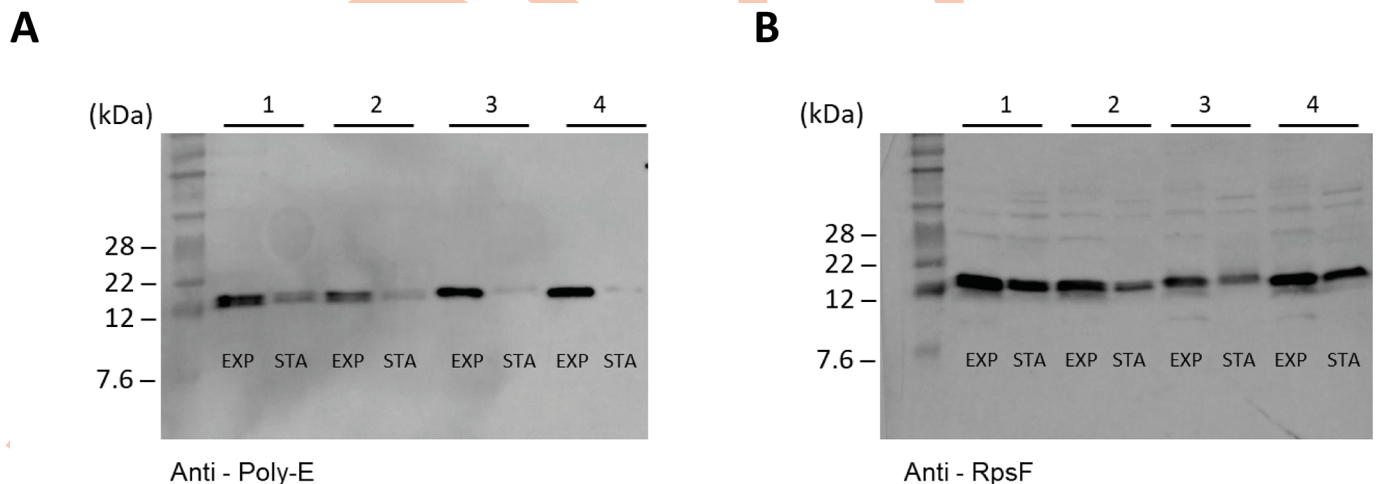


Fig 6. Proteolysis of RpsF glutamate tails is enhanced in stationary phase in a RimB-independent manner. (A) Western blot showing levels of RpsF_{10glu} in different genetic backgrounds. Panel 1, SBW25 *rpsF_{10glu}*; Panel 2, SBW25 Δ *rimK rpsF_{10glu}*; Panel 3, SBW25 Δ *rimB rpsF_{10glu}*; Panel 4, SBW25 Δ *rimBK rpsF_{10glu}*. (B) Western blot showing levels of RpsF protein. The genetic background of panels 1–4 is the same as given in (A). EXP denotes samples taken from exponentially growing cells; STA denotes samples taken from stationary phase cells.

<https://doi.org/10.1371/journal.pgen.1008837.g006>

rimK deletion on protein abundance under the activating conditions (Fig 7, S2 Table), with a substantial fraction of the SBW25 proteome shifting towards higher ratios in $\Delta rimK$ (Fig 7, and boxplot in S5 Fig). Proteins with ratios differing significantly ($p \leq 0.05$) by a factor ≥ 2 between WT and $\Delta rimK$ (located above or below the dashed lines) are coloured in red (up) and blue (down). Substantial agreement with the previously determined RimK regulon [19] could be observed (indicated by the green dots in Fig 8 representing significant differences) confirming that RimK exerts rapid control of the SBW25 proteome under nutrient-limiting conditions and low temperature.

The timeframe for the proteomic changes observed in our iTRAQ experiment was much too rapid to be a result of the production of new ribosomes [23], suggesting that the proteomic

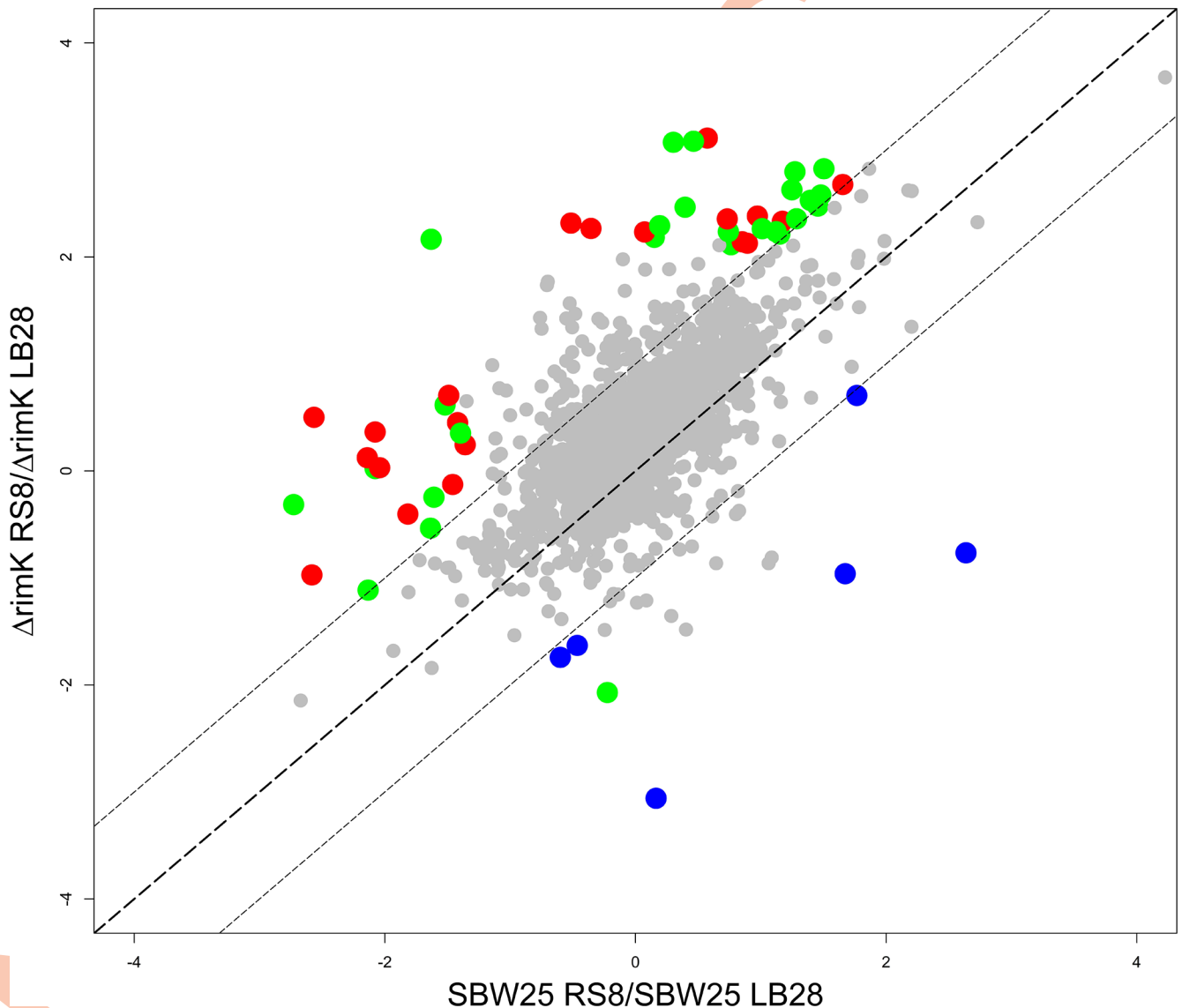


Fig 7. RimK activity rapidly affects the proteome of *P. fluorescens*. 2D scatter plot measuring \log_2 -fold change for condition A/condition B for WT on the X-axis and $\Delta rimK$ on the Y-axis. LB28 denotes 45 minutes incubation in LB medium at 28°C and RS8 denotes 45 minutes incubation in carbon-free rooting solution at 8°C. Proteins (filtered for at least unique 2 peptides) whose abundance is significantly (at least 2-fold difference of regulation between WT and $\Delta rimK$, at least one p -value ≤ 0.05) affected by *rimK* deletion are highlighted in red (upregulated) and blue (downregulated in $\Delta rimK$). Proteins differentially regulated and belonging to the previously determined RimK regulon [19] are highlighted in green.

<https://doi.org/10.1371/journal.pgen.1008837.g007>

changes we observe could represent an active response to modification of ribosomally-associated RpsF proteins.

RimABK exerts direct and indirect effects on mRNA translation through RpsF glutamation

Our data suggests that a large proportion of the observed *rimK* regulon is controlled through RimK-induced shifts in the abundance of other translational regulators, particularly Hfq [19]. To understand the contribution made by RimK glutamation to ribosome function, we must first understand the relationship between Hfq abundance and RimK. To assess the contribution of Hfq to the RimK phenotype, we produced *rimK* mutant strains in which the chromosomal *hfq* gene was flag-tagged at the C-terminus. We then quantified Hfq abundance using a Wes Simple Western system (Bio-Techne) in different media conditions. As expected based on previous results [19], Hfq abundance decreased markedly in the $\Delta rimK$ background for cells grown in M9-pyruvate media. This reduction in Hfq levels was observed for cells grown to early exponential or to stationary phase. Interestingly, the relationship between RimK and Hfq was reversed for cells grown in M9-pyruvate supplemented with Cas-aminoacids. Under these conditions, *rimK* deletion led to a noticeable increase in Hfq abundance in early exponential phase (Fig 8). The results obtained for stationary phase growth in M9-pyr-Cas followed the same trend, with one $\Delta rimK$ sample showing an increase in Hfq and the second showing little change. This may reflect the depletion of one or more amino-acid sources in the second sample.

Based on these data, we expect that much of the effect of *rim* gene deletion on the SBW25 translome would be reversed for cells grown with Cas-aminoacids as opposed to with pyruvate alone. To test this, we conducted a Ribo-seq analysis on SBW25 WT and $\Delta rimBK$ cells grown to early exponential phase in M9-pyr-Cas media. The translational activity of 806 genes was significantly ($\log_2 > 1$) affected by *rimBK* deletion (S3 Table), with more affected genes showing reduced (564) than increased (242) mRNA abundance in the $\Delta rimBK$ mutant

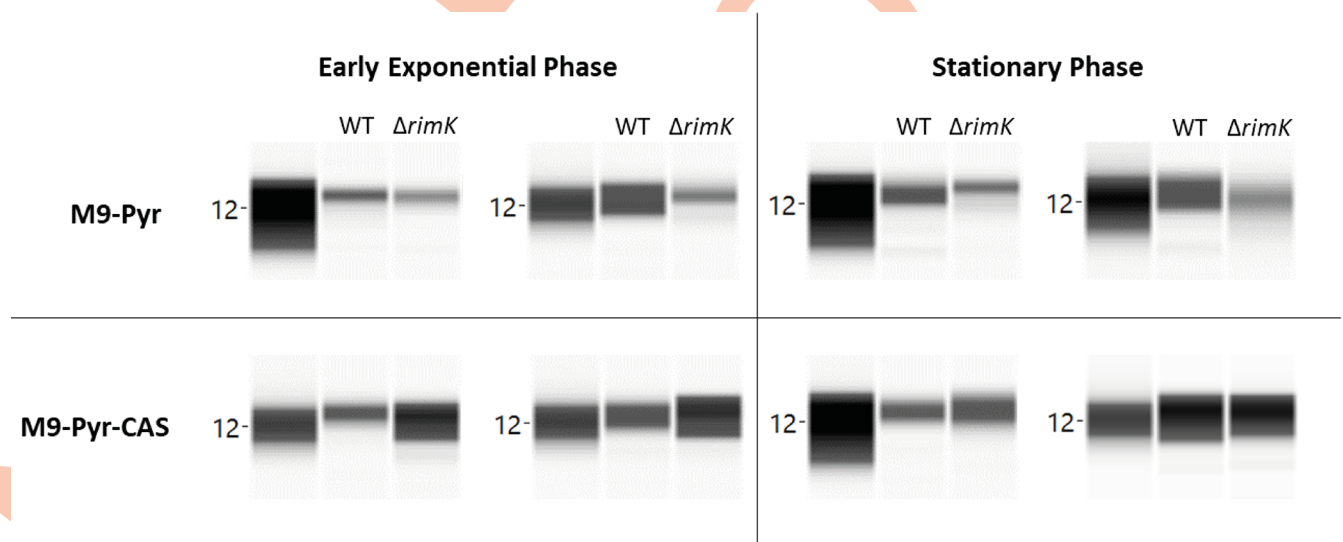


Fig 8. The influence of RimK on Hfq abundance is dependent upon media conditions. SBW25 WT or $\Delta rimK$ cells were grown in either M9-pyruvate (abbreviated M9-Pyr) or M9-pyruvate with Cas-aminoacids (abbreviated M9-Pyr-CAS) to either early exponential phase or stationary phase as indicated. Each panel shows two biological duplicates; in each case the 12KDa molecular weight marker is shown (Hfq-FLAG has a predicted molecular weight of 12.04 KDa).

<https://doi.org/10.1371/journal.pgen.1008837.g008>

background. The upregulated *rimBK* regulon was dominated by ribosomal proteins, while the downregulated genes contained a large proportion of ABC amino-acid transporter subunits. We observed a large degree of overlap between this experiment and our published data for the *rimK* proteome [19], with many upregulated genes in the initial (M9-pyr, stationary phase) experiment downregulated in our Ribo-seq dataset and *vice versa* (S3 Table).

Our data indicate that RimK produces an indirect, nutrient-dependent effect on the SBW25 translome by changing the intracellular abundance of Hfq. To test whether RpsF glutamation also exerts a direct effect on SBW25 gene translation, we produced an additional $\Delta rimBK$ mutant strain in which the *rpsF* gene was extended by 4 glutamate residues. The $\Delta rimBK rpsF_{4glu}$ mutant proved extremely difficult to produce, with the eventual mutant strain displaying a complete loss of UV fluorescent siderophore secretion compared to WT SBW25 (S3 Fig). Subsequent whole genome sequencing of this mutant revealed additional SNPs in the *pvdI* and *pvdJ* pyoverdinin biosynthetic loci. To investigate the potential significance of these *pvdIJ* mutation we grew SBW25 WT, $\Delta rimBK$ and $\Delta rimBK rpsF_{4glu}$ strains on KB Congo Red plates containing excess $FeCl_2$ to repress pyoverdinin production. Under these conditions the $\Delta rimBK rpsF_{4glu}$ mutant displayed enhanced Congo Red binding compared to WT and $\Delta rimBK$, suggesting that the *rpsF_{4glu}* mutation exerts a *rimBK/pvdIJ*-independent effect on SBW25 physiology (S3 Fig).

Both $\Delta rimBK rpsF_{4glu}$ and $\Delta rimBK rpsF_{10glu}$ mutants showed a pronounced swarming motility defect compared with WT SBW25 and $\Delta rimBK$, while the $\Delta rimBK rpsF_{4glu}$ strain also displayed a significant increase in Congo Red binding. Growth of neither strain was affected in rich (KB) or poor (M9-pyr) media (S4 Fig). To investigate the molecular basis of the *rpsF_{4glu}/10glu* phenotypes, we conducted Ribo-seq assays for $\Delta rimBK rpsF_{4glu/10glu}$ and compared these data to the translome of $\Delta rimBK$. Translational activity of 159 genes was significantly ($>1.0 \log_2$) affected by the *rpsF_{4glu}* mutation (Fig 9, S4 Table), with roughly equal numbers of up- (79) and downregulated (80) genes. Consistent with the observed preference of the RimBK system to produce RpsF_{4glu} ribosomal variants (Fig 4), the *rpsF_{10glu}* mutation affected considerably fewer gene targets, with ribosomal activity differing significantly from the $\Delta rimBK$ background for only 45 loci (S7 Fig, S4 Table). By comparing the significantly affected genes for $\Delta rimBK$ /WT against the results for $\Delta rimBK rpsF_{4glu}/\Delta rimBK$, we were able to identify three distinct subgroups of loci within the *rpsF_{10glu/4glu}* translomes. The first of these were genes whose translation is altered by *rimBK* deletion, but not by RpsF glutamation (Class 1, Fig 9B). These genes comprised the majority of the *rimBK* regulon, and overlapped substantially with our previously published Hfq translome dataset [7]. Translation of the second set of genes (Class 2, Fig 9C) was shifted by RpsF glutamation and *rimBK* deletion in the same direction (usually downregulated). This set contained numerous small, uncharacterised proteins alongside several stress response proteins and amino-acid ABC transporters/ metabolic genes (S5 Table). We observed a large degree of overlap with the equivalent dataset for RpsF_{10glu}, suggesting that both mutations produce similar effects on this gene class.

The third set of genes (Class 3, Fig 9D); those inversely affected by RpsF glutamation and *rimBK* deletion, are candidates for the direct RpsF-glutamation regulon. For RpsF_{4glu}, these genes predominantly split into four main classes (S5 Table): ABC transporters for fatty/amino-acids, metabolic pathways for metabolism of amino acids, and genes associated with the initial stages of attachment to surfaces (e.g. pili and curli biosynthesis loci) were upregulated by glutamation. As predicted based on the *pvdIJ* mutation, downregulated loci also included the ferri-pyoverdinin receptor *fpvA* [24]. RimBK regulation of these key groups (fatty/amino acid transport and metabolism, initial surface attachment and secretion of macromolecules) was also seen when we extended our analysis to include genes that were less than 2-fold different in $\Delta rimBK$ versus WT, but more than 2-fold inversely affected in *rpsF_{4glu}* (S5 Table, Fig 9E). This

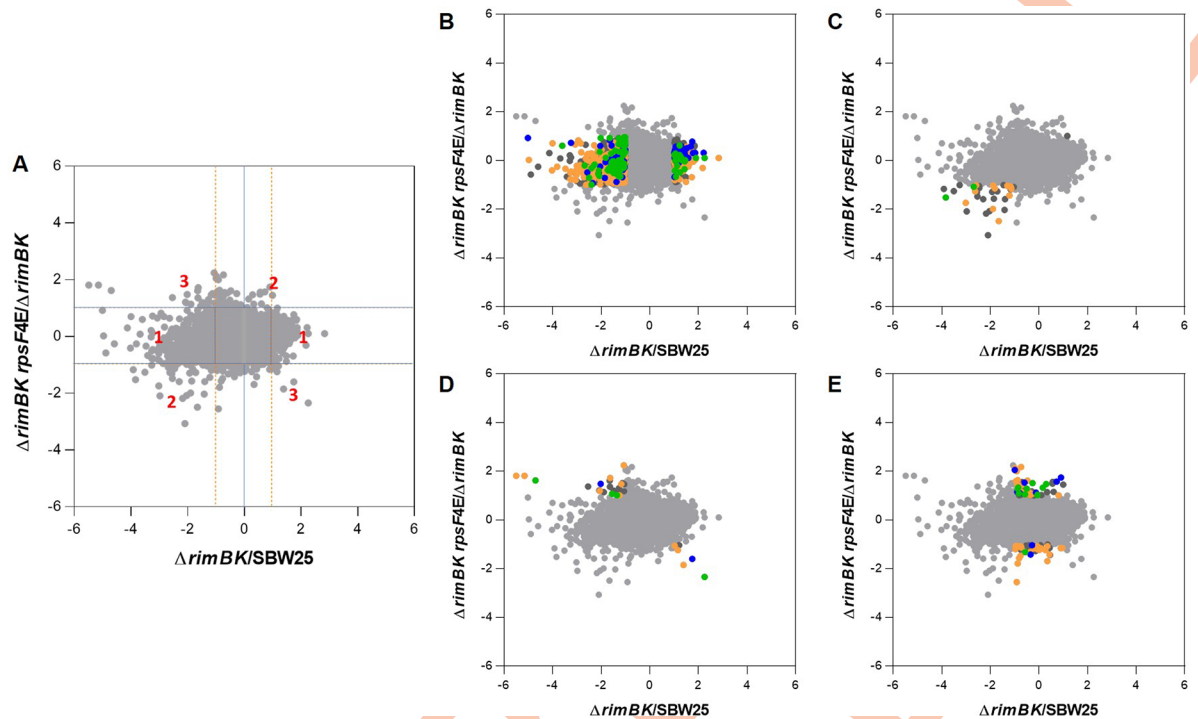


Fig 9. Scatterplots representing the pairwise comparisons of \log_2 ratios between the $\Delta rimBK rpsF_{4glu}$ and $\Delta rimBK$ translomes. (A) Location of class 1, class 2 and class 3 genes are indicated. Horizontal and orange dashed vertical lines indicate regions of $>1.0 \log_2$ deviation from zero. **(B-D)** Highlighted regions containing class 1, 2 and 3 genes respectively. **(E)** Genes significantly ($>1.0 \log_2$) affected by *rpsF* glutamation but not significantly affected by *rimBK* deletion. Highlighted genes are listed in S4 Table and colour-coded according to their COG classifications: yellow = metabolism; green = cellular processes and signalling; blue = information storage and processing; dark grey = poorly characterised.

<https://doi.org/10.1371/journal.pgen.1008837.g009>

group contained loci for pectate lyase and phytase secretion (both upregulated by glutamation), alongside loci linked to regulation of motility and surface attachment [25]. We saw little overlap between the *RpsfF*_{4glu} and *RpsfF*_{10glu} regulons for this group of genes, with the smaller, less well-defined 10E regulon containing a few ABC transporter components alongside several hypothetical proteins (S5 Table).

Discussion

Bacterial adaptation to complex natural environments is controlled by an intricate series of connected signalling pathways that function both within individual cells and on the microbial community as a whole [11, 14, 26]. In addition to extensive transcriptional [6, 11] and protein functional regulation [12], control of mRNA translation is critical for effective colonisation of plant rhizospheres [7]. In this study we characterise the RimABK pathway in *Pseudomonas fluorescens* and present evidence for the role that this novel translational regulatory system plays during bacterial adaptation to the rhizosphere environment through specific, controlled modification of a ribosomal protein.

The activity of the RimK glutamate ligase is controlled by several distinct environmental inputs and the intracellular levels of key molecules. At the transcriptional level, expression of the polycistronic *rimABK* mRNA is controlled by temperature and nutrient availability, with cold, nutrient-starved conditions leading to increased *rim* transcript abundance. At this stage the transcriptional regulators that control *rim* expression are unknown. The environmental cues that activate *rim* transcription would make the operon a plausible target for σ^S regulation,

although this was not supported by a recent study of sigma-factor regulation in *P. aeruginosa* [27]. A further, substantial fraction of RimK regulation occurs at the protein activity level, where RimA, RimB and intracellular levels of glutamate and cdG combine to translate a complex set of environmental variables into the proportion of all ribosomally-associated RpsF proteins that have C-terminal poly-glutamate tails.

Our results suggest that in the presence of RpsF, RimK adds glutamate units and RimB removes them. The length of poly-glutamate tails is restricted, tending towards a minimal number of 4, as a consequence of the specific protease activity of RimB. With low levels of cdG in the system, a balance is established where RimK activity predominates and a range of chain lengths (longer than four) arises. This may also reduce the fraction of RpsF proteins that can be glutamated. In the presence of RimB and with increasing cdG levels, RimA activity switches from its default role of stimulating RimK to degrading cdG, leading to a reduction in RimK activity and an increased ratio of RimB to RimK activity (S8 Fig). RimA thus functions as a cdG-trigger enzyme [28]: a signalling protein whose enzymatic activity changes its interaction with a regulatory partner, in this case RimK. The data showing that both RimA and cdG increase RimK ATPase and glutamate ligase activity when no RimB is in the system, suggests that this trigger behaviour of RimA requires the presence of RimB. The kinetic details of this mechanism remain unclear.

The cdG-induced switch of RimA activity results in shortened RpsF chain lengths and higher overall coverage. RimA phosphodiesterase activity may also serve to dampen the effect of transient fluctuations in cdG level on RimK activity. Short impulses of cdG would be rapidly degraded by RimA and RimK activity would quickly return to the default position of making longer chains. Only if cdG is produced and present in sufficient quantities for a defined time would RimK glutamation activity drop, thus enabling RimB to limit RpsF chain lengths and move towards global RpsF coverage. The trade-off between long chains and high RpsF coverage is therefore determined by cdG availability. To enable RpsF modification to function as an effective regulator, a mechanism should also exist to return modified RpsF to a non-glutamated 'ground state' (Fig 6). Our conceptual model for Rim function is summarised in Fig 10.

The proportion of modified versus unmodified RpsF proteins leads to altered proteome composition and translational activity, which can be effectively measured using Ribo-seq. This sequencing-led approach measures global ribosomal activity towards different mRNAs. We have previously shown that Ribo-seq provides a more accurate assessment of translational regulation than either RNA-seq, which does not record translation level control, or quantitative proteomic analyses that are subject to extensive, compensatory post-translational effects [7]. The implications of Rim activity are substantial, with the translation of several hundred genes significantly affected in a $\Delta rimK$ mutant strain.

Much of the altered translational activity in $\Delta rimK$ can be explained by changes in Hfq abundance. Consistent with this, the mobile tails of RpsF and the neighbouring ribosomal protein S18 have been shown to stochastically interact with protein S1 in the *E. coli* ribosome [29]. Protein S1 is required for translation initiation of mRNAs with structured 5' ends or with weak or no Shine-Dalgarno sequences [30]. Furthermore, in *E. coli* S1 weakly and reversibly associates with the ribosome and interacts with Hfq when binding RNA polymerase to affect transcription [31]. In *P. aeruginosa*, Hfq interaction with nascent transcripts has been proposed as a mechanism for controlling translation in cases where transcription and translation are coupled [32]. Additionally, Hfq has been shown to associate with *E. coli* ribosomes, and both Hfq and S1 are components of the bacteriophage Q β replication complex [33–35]. It is possible therefore that modification of RpsF by C-terminal glutamation may disturb the binding equilibrium between protein S1 and the ribosome, influencing the cellular localisation of S1 and Hfq. A redistribution of S1 and Hfq within the cell would be expected to exert a

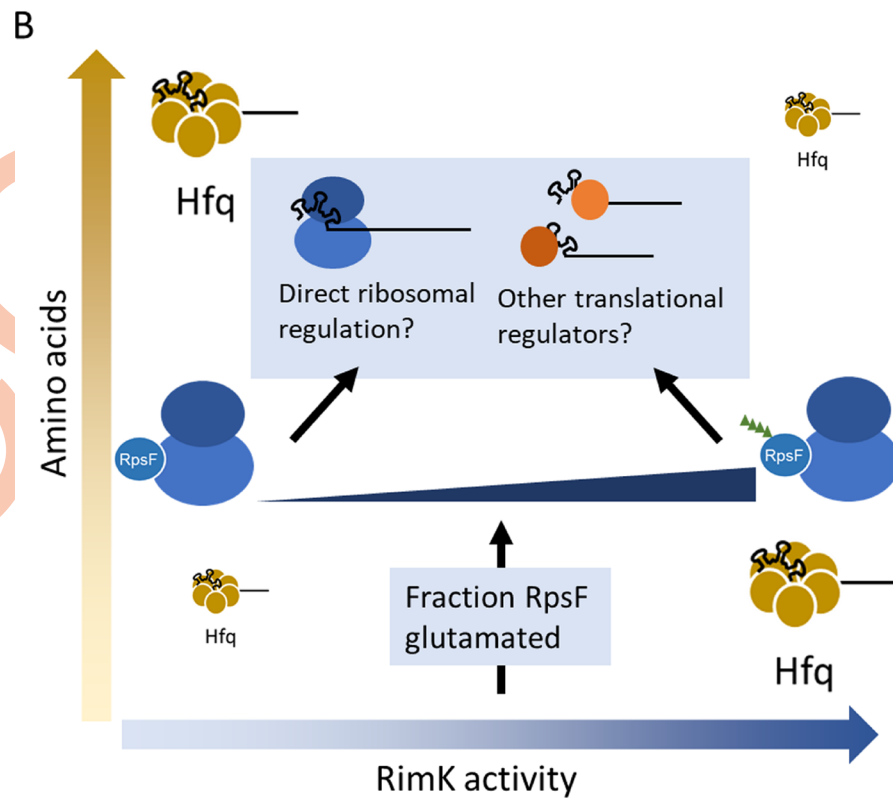
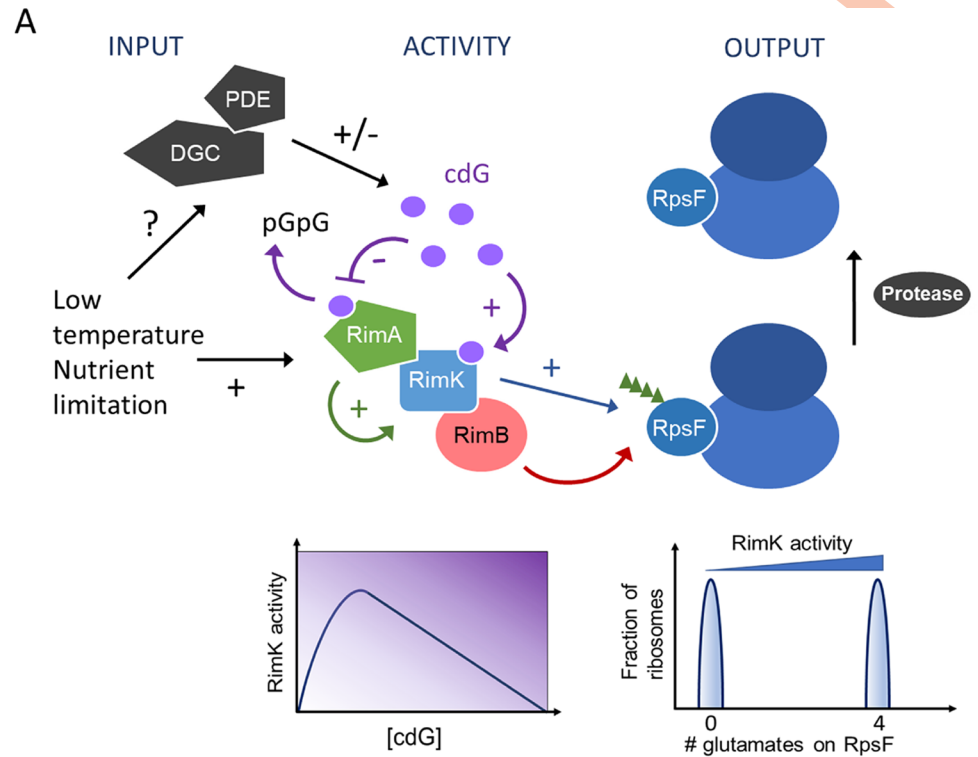


Fig 10. A model for RimABK/RpsF regulation in *P. fluorescens*. Activity of RimK (blue rectangle) is stimulated by direct interaction with RimA (green pentangle) and cdG (purple circles). CdG also interacts with RimA, leading to its hydrolysis to the linear dinucleotide pGpG and an accompanying loss of RimA stimulation. The combined activity of the glutamate ligase RimK and the poly-glutamate protease RimB (red oval) adds chains of ~4 glutamate residues (green triangles) to the C-terminus of ribosomal protein RpsF (blue oval). Known inputs to the system include changes in *rimABK* expression, stimulated by low temperature and nutrient limitation, glutamate concentration, and cdG concentration. CdG levels are controlled in turn by as-yet-unknown diguanylate cyclases/phosphodiesterases (grey pentangles). These inputs combine to control the proportion of glutamated ribosomes in the cell. Glutamated ribosomes are returned to a non-glutamated state by the action of an as-yet-unknown protease (grey oval). Insets below the main diagram illustrate the impact of increasing cdG concentration on RimK activity (left, Fig 3, S6 Fig) and the predicted relationship between RimK activity and ribosomal glutamation (right, Fig 5B). (B) Model for Rim system function in high and low concentrations of amino acids. While the Rim system affects ribosome glutamation, and subsequent mRNA translation according to the model shown in 10A, the effect of the Rim system on Hfq abundance is strongly dependent on the nutrient status of the environment. This results in a regulatory output that varies in response to both RimK activity (itself controlled by cdG) and amino-acid abundance.

<https://doi.org/10.1371/journal.pgen.1008837.g010>

significant effect on protein abundance and may explain a substantial fraction of the observed RimK regulatory activity that is not mediated by the glutamation of RpsF (Fig 9).

While RimK disruption or RpsF modification both affect the *P. fluorescens* proteome, the addition of four glutamate residues to RpsF has additional biological significance. Strains with the *rpsF*_{4glu} allele display a shift in translational activity for a set of genes associated with early-stage surface attachment, amino-acid utilisation and transport and the secretion of molecules (e.g. phytase and pectate lyase) associated with rhizosphere colonisation. RpsF modification specifically affects translation and proteome composition within minutes of detecting an environmental shift. This strongly suggests that glutamation by RimK is not a passive process determining long-term population level adaptation, but rather is an active mechanism used by individual cells to rapidly adapt to changes in their environments by modifying mRNA translation activity.

We are now able to propose a general mechanism for RimK translational control (Fig 10). Nonetheless, several key questions remain to be answered. Firstly, the exact mechanism of translational discrimination by ribosomes containing modified and unmodified RpsF is still unclear. It remains to be determined whether the observed effect on mRNA translation is direct (i.e. through altered ribosome function) or if it functions through an as yet uncharacterised indirect mechanism (e.g. via altered levels of an unidentified translational regulator or through interaction with other affected target proteins/RNAs). We were unable to identify any clear distinguishing features in the primary or predicted secondary structures of the Rim-regulated mRNAs, nor could we assign them definitively to a single transcriptional or translational regulon. Thus, at this stage, several indirect options that could confer selectivity to the ribosome remain to be evaluated. Given the highly pleiotropic effects of *rim* gene disruption, the mechanism of RpsF-discrimination likely awaits a comparative structural analysis of modified and unmodified *Pseudomonas* ribosomes. More generally, the identity of several important pathway components; specifically, the 'reset' protease that removes 4E tails from RpsF, and the DGCs/PDEs that control the cdG input to RimA/RimK remain to be determined. These proteins present additional opportunities for regulatory input to the Rim pathway, increasing the complexity of the system and further integrating it into the signalling network that controls *Pseudomonas* behaviour.

Finally, a comparative examination of the Rim proteins from different bacterial species may provide interesting new insights into the function and biological significance of the RimABK pathway and its individual component proteins. RimK homologs have been linked to stress-tolerance and pathogenicity in several human and plant pathogens [19, 36], although the phenotypic consequences of *rimK* deletion vary widely between different organisms [19]. Furthermore, variations on the classical three-gene Rim pathway are widespread in nature, with RimBK, RimAK and RimK-only variants identified in diverse bacterial families. Homologs of

rimK have also been identified in several eukaryotic genomes. Overall, our study suggests that dynamic, post-translational ribosomal modification is a common feature of prokaryotic, and potentially archaeal and eukaryotic environmental adaptation.

Materials and methods

Strains and growth conditions

Plasmids and strains are listed in [S6 Table](#). Primers are listed in [S7 Table](#). Unless otherwise stated all *P. fluorescens* strains were grown at 28°C and *E. coli* at 37°C in lysogenic broth (LB) [37] solidified with 1.3% agar where appropriate. Gentamycin was used at 25 µg/ml, carbenicillin at 100 µg/ml, and tetracycline (Tet) at 12.5 µg/ml. For inducible plasmids, IPTG was added to a final concentration 0.2 mM (SBW25) or 1 mM (*E. coli*), unless otherwise stated.

Molecular microbiology procedures

Cloning was carried out in accordance with standard molecular microbiology techniques. The pETM11-*rpsF*_{10^{glu}}, pETM11-*rimA*_{E47A} and *E. coli rpsF* purification vectors were produced by ligating PCR fragments (amplified with primers 17/18, 11/12/15/16 and 13/14 respectively) between the *Nde*I and *Xho*I sites of plasmid pETNdeM-11 [38] as appropriate. Purification vectors for *rimA*, *rimB* and *rimK* were as described in [19] using primers 7–12. *P. fluorescens* SBW25 site-specific mutants were constructed using a modification of the protocol described elsewhere [39]. Up- and downstream flanking regions to the target modification site (*rimBK*, *hfq* or *rpsF*) were amplified using primers 19–25, 26–31 and 32–37 respectively. PCR products in each case were ligated into pTS1 between *Kpn*I/*Eco*RI, *Nde*I/*Bam*HI and *Xho*I/*Kpn*I respectively. The resulting vectors were transformed into the target strain, and single crossovers were selected on Tet and re-streaked for single colonies. Cultures from single crossovers were grown overnight in LB medium, then a dilution series plated onto LB plates containing 5% w/v sucrose to enable *sacB* counterselection. Individual sucrose-resistant colonies were patched onto LB plates ± Tet, and Tet-sensitive colonies tested for successful gene modification by colony PCR followed by Sanger sequencing. Reverse transcriptase PCR (RT-PCR) and 5' RACE were conducted using primers (1/2 and 3/4 respectively). qRT-PCR was performed as described in [19] using primers 5/6. qRT-PCR experiments were repeated three times independently and data are presented +/- standard error.

Purification of Rim and RpsF proteins

Protein purification was conducted after [19]. Briefly, overnight cultures of *E. coli* BL21-(DE3) pLysS were used to inoculate 1.0 litre overexpression cultures. These were then grown at 30°C to an OD₆₀₀ of 0.6, before protein expression was induced for 2 hours with 1mM IPTG. Cells were lysed using a cell disruptor (Avestin) and His₆-tagged proteins purified by NTA-Ni chromatography. 1 ml HiTrap chelating HP columns (Amersham) were equilibrated with 25 mM KH₂PO₄, 200 mM NaCl, pH 8.0 (SBW25 RimA/B/K), 50 mM Tris-Cl, 2.5% glycerol, pH 8.0 (SBW25 RpsF) or 50 mM Tris, 300 mM NaCl, 10 mM imidazole, pH 9.0 (*E. coli* RpsF), and loaded with cell lysate. Following protein immobilization, proteins were eluted with a linear gradient to 500 mM imidazole over a 15 ml elution volume.

Linked pyruvate kinase / lactate dehydrogenase (PK/LDH) ATPase activity assays

ATPase activity was measured indirectly by monitoring NADH oxidation in a microplate spectrophotometer (BioTek Instruments) at 25°C. The reaction buffer consisted of 100 mM

Tris-Cl (pH 9.0), 20 mM MgSO₄. Each 100 μL reaction contained 0.4 mM NADH, 0.8 mM phosphoenolpyruvic acid, 0.7 μL PK/LDH (Sigma) and was initiated by the addition of 10 μL ATP. Protein concentrations were as shown in the figure legends. Enzyme kinetics were determined by measuring A₃₄₀ at 1-minute intervals. Kinetic parameters were calculated by plotting the specific activity of the enzyme (nmol ATP hydrolyzed/min/mg protein) versus ATP concentration and by fitting the non-linear enzyme kinetics model (Michaelis-Menten) in Graph-Pad Prism. 25 μM cyclic dinucleotides were included where appropriate, as noted in the text.

RpsF glutamation and protease assays

The glutamation assay was adapted from [22]. Briefly, purified RpsF and Rim proteins at the concentrations indicated in the figure legend were incubated at room temperature for the indicated times in reaction buffer comprising 100 mM Tris-HCl pH 9.0, 20 mM L-glutamate (unless otherwise indicated), 20 mM ATP and 20 mM MgSO₄·7H₂O. Reactions were supplemented with cdG (Sigma) as indicated in the text. Protease assays were performed in 100 mM TRIS-HCl pH 9.0, 20 mM L-glutamate, 20 mM ATP, 20 mM MgSO₄·7H₂O with RimB concentrations as stated in the figure legend. For both experiments, samples were boiled in SDS loading buffer and analyzed by SDS-PAGE following completion of the reaction.

Growth assays

Bacterial growth was measured in a microplate spectrometer (BMG Labtech FLUOstar Omega) using 2 biological duplicates each providing 2 experimental replicates and are presented as mean +/- standard error. 150 μL of the indicated growth medium in each case was added to the internal 60 wells of clear-bottomed, black-walled 96-well microplates (Sigma). Carbon sources were added to a concentration of 0.4% w/v in each case. Growth was initiated by the addition of 5 μL of overnight cell culture (LB media, 28°C, shaking) normalized to an OD₆₀₀ of 0.01. Plates were incubated statically at 28°C and agitated immediately prior to each data acquisition step. Optical density was measured at 600nm and fluorescence was monitored at 460nm with an excitation wavelength of 355nm. Experiments were conducted at least twice independently.

Phenotypic assays

To assess the colony morphology of the SBW25 *rim/rpsF* mutants, Kings B (KB) plates [40] were prepared containing 0.8% w/v agar, 1% w/v NaCl, 0.004% Congo Red dye, +/- 100 μM FeCl₂. Plates were allowed to dry for 45 min in a sterile flow chamber. Meanwhile SBW25 strains were grown over-day at 28°C in LB media with shaking. Cell densities were adjusted to give an optical density (λ 600nm) of 0.2 then 1.5 μL of each culture was spotted onto the media surface. Six replicates were prepared from two biological duplicates (three plates prepared from each). Plates were then incubated at 28°C for the time indicated in the figure legends before photographing, with a representative image shown in each case.

To quantify swarming diameter, Kings B (KB) media plates containing 0.3% agar w/v, 1% w/v NaCl, 0.004% Congo Red dye were produced and allowed to set and dry for 45 min in a sterile flow chamber. SBW25 strains were grown overnight at 28°C in LB media with shaking. The following morning, cell densities were adjusted to an optical density (λ 600nm) of 0.2 then 5 μL of each culture was spotted onto the media surface. Six replicates were prepared from two biological duplicates (three plates prepared from each). Plates were then incubated over-day at 28°C then overnight at 4°C before photographing, with a representative image shown in each case. All phenotypic experiments were conducted at least twice independently.

Determining the transcription start site of the *rim* operon

5' RACE (Life Technologies) was performed on mRNA prepared from SBW25 cells grown overnight in M9 media with pyruvate (0.4% w/v) as sole carbon source. RNA was purified by column capture (Qiagen RNeasy Mini Kit). Purified RNA was subjected to additional DNase treatment (Turbo DNase, Ambion). The final PCR product from the 5' RACE procedure was excised from a 1% agarose gel and purified by column capture (Macherey-Nagel Nucleospin mini kit). The purified product was then Sanger sequenced (Eurofins Scientific) to reveal the position of the transcriptional start site.

RT-PCR

cDNA from SBW25 cells was prepared as an independent step prior to PCR. Total RNA was extracted from cells grown in M9 media containing pyruvate (0.4% w/v) as sole carbon source by column capture (Qiagen RNeasy Mini Kit). Purified RNA was subjected to additional DNase treatment (Turbo DNase, Ambion). The resulting RNA was then subjected to amplification (Merck WTA2 Amplification Kit) to produce cDNA that was subsequently purified by column capture (Qiagen QiaQuick PCR purification kit) and eluted in RNase-free water. PCR was performed on the cDNA using high-fidelity DNA polymerase (New England Biolabs Phusion polymerase) using a forward primer targeting the start of *rimA* (*PFLU0263*) and a reverse primer targeting the end of *rimK* (*PFLU0261*). The resulting PCR product was purified by column capture (Macherey-Nagel Nucleospin mini kit) and sequenced (Eurofins Scientific) to confirm the presence of the three *rim* genes.

Ribosome preparation for automated immunodetection

50ml LB cultures were grown overnight at 28°C. Cultures were pelleted by centrifugation and resuspended into either 35ml LB media at 28°C or Rooting Solution (RS) at 4°C. Samples were subsequently incubated in the stated condition for 45 minutes. Crude ribosomes were prepared according to (64). In brief, cells were pelleted at either 28°C or 4°C according to the temperature at which they had been incubated. Pellets were resuspended into 15 ml Buffer A (20 mM Tris pH 7.5, 300 mM NH₄Cl, 10 mM MgCl₂, 0.5 mM EDTA, 6 mM β-mercaptoethanol (β-ME), 10 units/ml SuperASE-In (Ambion) + 0.1mM PMSF pre-equilibrated to the appropriate temperature. Cells were lysed using a cell disruptor (Avestin). Samples were made up to 35 ml using Buffer A and centrifuged at 30,000 x g for 50 minutes. 27 mls of sample was carefully withdrawn and centrifuged at 100,000 x g for 1 hour. The resulting crude ribosome pellet was rinsed with Buffer A and resuspended into 100 μL 50 mM Tris pH 8.0, 50mM NaCl.

Automated immunodetection

Biological duplicate SBW25 cultures were grown overnight in LB media at 28°C. These cultures were used to inoculate 50ml volumes of M9-pyruvate minimal media, with and without Cas-aminoacids. Pyruvate and Cas-aminoacids were used at a concentration of 0.4% w/v. When cultures reached an optical density of 0.3 (measured at 600 nm), 1 ml of culture was removed, centrifuged and the resulting pellet resuspended into 100 μL supernatant + 100 μL x2 SDS loading buffer. The remaining cultures were allowed to grow overnight to reach stationary phase. 150 μL of a WT culture grown in M9-Pyr-CAS was taken and a proportionate volume of all other cultures (according to differences in optical density measured at 600nm) was taken. Pellets were resuspended as above. Prior to immunodetection, samples were briefly sonicated to reduce viscosity. For the detection of Hfq, 0.5 μL of each sample was run on WES ProteinSimple automated immunodetection system (Bio-Techne) according to the

manufacturer's instructions. For the detection of RpsF, following ribosome preparation, 1 μ L sample derived from cells grown in LB media at 28°C and 2 μ L sample derived from cells grown in RS at 4°C was run on the same instrument.

Western blotting

Following growth in M9-Pyr-CAS, the concentration of the soluble protein fraction from SBW25 cells was normalized. 140 μ g total protein from each sample was loaded in a 25 μ L volume onto one of two SDS-PAGE gels. Gels were blotted onto polyvinylidene difluoride (PVDF) membranes (Millipore). Membranes were incubated overnight in blocking solution (1x PBS pH 7.4, 0.01% Tween 20, 5% milk powder). Protein was subsequently detected with either 1/2000 anti-polyglutamate chain (AdipoGen) or 1/200 anti-RpsF (Dundee Cell Products) antibodies and 1/6000 anti-rabbit secondary antibody (Sigma). Bound antibody was visualized using ECL chemiluminescent detection reagent (GE Healthcare).

Protein extraction and mass spectrometry

SDS gel slices containing protein samples of interest were washed, treated with DTT and iodoacetamide, and digested with trypsin according to standard procedures. Peptides were extracted from the gels and analysed by LC-MS/MS on an Orbitrap-Fusion mass spectrometer (Thermo Fisher, Hemel Hempstead, UK) equipped with an UltiMate 3000 RSLCnano System using an Acclaim PepMap C18 column (2 μ m, 75 μ m x 500mm, Thermo). Aliquots of the tryptic digests were loaded and trapped using a pre-column which was then switched in-line to the analytical column for separation. Peptides were separated using a gradient of acetonitrile at a flow rate of 0.25 μ L min⁻¹ with the following steps of solvents A (water, 0.1% formic acid) and B (80% acetonitrile, 0.15% formic acid): 0–3 min 3% B (trap only); 3–4 min increase B to 7%; 5–40 min increase B to 50%; 40–45 min increase B to 65%; followed by a ramp to 99% B and re-equilibration to 3% B.

Data dependent analysis was performed using HCD fragmentation with the following parameters: positive ion mode, orbitrap MS resolution = 120k, mass range (quadrupole) = 300–1800 m/z, MS2 top20 in ion trap, threshold 1.5e⁴, isolation window 1.6 Da, charge states 2–7, AGC target 2e⁴, max inject time 35 ms, dynamic exclusion 1 count, 15 s exclusion, exclusion mass window \pm 5 ppm. MS scans were saved in profile mode and MS2 scans were saved in centroid mode.

To generate recalibrated peaklists, MaxQuant 1.6.0.16 was used, and the database search was performed with the generated HCD peak lists using Mascot 2.4.1 (Matrixscience, UK). The search was performed on a *Pseudomonas fluorescens* SBW25 protein database (Uniprot, 20140727, 21,935 sequences) to which copies of the RpsF sequence with 1–10 additional glutamate residues (E) at the C-terminus was added. For the search a precursor tolerance of 6 ppm and a fragment tolerance of 0.6 Da was used. The enzyme was set to trypsin/P with a maximum of 2 allowed missed cleavages. Oxidation (M), deamidation (N, Q), and acetylation (N-terminus) were set as variable modifications, carbamido-methylation (CAM) of cysteine as fixed modification. The Mascot search results were imported into Scaffold 4.4.1.1 (www.proteomsoftware.com) using identification probabilities of 99% for proteins and 95% or 0% for peptides, as discussed in the results. The mass spectrometry proteomics data have been deposited to the ProteomeXchange Consortium via the PRIDE [41] partner repository with the dataset identifier PXD017233.

Quantitative mass spectrometric analysis using isobaric labelling (iTRAQ)

50 ml overnight cultures of SBW25 WT and $\Delta rimK$ were grown at 28°C in LB medium with shaking. Cultures were then pelleted by centrifugation and resuspended in equal volumes of A) carbon-free rooting solution [19], pre-cooled to 8°C, and B) LB medium, pre-heated to 28°C. Cultures were incubated for 45 minutes with shaking at 8 or 28°C as appropriate, then cellular activity was halted by addition of 30 ml of RNeasy lysis buffer [saturated $(NH_4)_2SO_4$, 16.7 mM Na-Citrate, 13.3 mM EDTA, pH 5.2] containing protease inhibitors. Cell samples were then pelleted, washed three times with 10 mM HEPES pH 8.0 + protease inhibitors, before re-suspension to a final volume of 200 μ L. 700 μ L pre-cooled RLT + β -mercaptoethanol buffer (RNeasy Mini Kit, QIAGEN) was added and samples lysed with two 30 s Ribolyser pulses at speed setting 6.5. Supernatant was removed, and the soluble fractions separated by ultracentrifugation (279,000 g, 30 min, 4°C).

After determination of protein concentration, the soluble proteins were precipitated with chloroform-methanol and subjected to iTRAQ 4-plex quantification. The experiment was performed with 2 biological replicates. In each replicate the samples were labelled with an iTRAQ 4 plex kit (Sciex) as follows: 114 = WT LB28, 115 = $\Delta rimK$ LB28, 116 = WT RS8, 117 = $\Delta rimK$ RS8. The labelled samples were combined and fractionated using the Pierce High pH Reversed-Phase Peptide Fractionation Kit producing 7–8 fractions. After analysis on an Orbitrap Fusion (Thermo) using MS3 synchronous precursor selection based on methods described previously [7], the raw data from both replicates were combined and processed in Proteome Discoverer 2.4 (Thermo) with the following main parameters: protein sequence database: *P. fluorescens* SBW25 (Uniprot, Feb/2016, 6388 entries); variable modifications: oxidation (M), deamidation (N,Q); Percolator strict FDR target: 0.01; reporter ion quantifier: most confident centroid, 20 ppm, HCD, MS3; consensus workflow for statistical analysis: replicates with nested design; use unique peptides for protein groups only, co-isolation threshold 50%, imputation: low abundance resampling, ratio based on pairwise ratios, hypothesis test: t-test (background based) generating adjusted p-values according to Benjamini-Hochberg. The protein results table was exported from Proteome Discoverer and used to generate the final protein expression tables and plots (Fig 7, S5 Fig and S2 Table) in The R Project for Statistical Computing.

Ribosomal profiling (Ribo-Seq) analysis

Ribosomal profiling was conducted as described in [7]. SBW25 cultures were grown at 28°C in M9-pyr-CAS medium to the late exponential phase, then cells were harvested by rapid filtration as described in [42]. Collected cells were flash frozen in liquid nitrogen and cryogenically pulverized by mixer milling (Retsch), then thawed and clarified by centrifugation. Resulting lysates were digested with MNase, quenched with EGTA and resolved by sucrose density gradient ultracentrifugation. Ribosome-protected mRNA footprints were processed as previously described [7, 42] and sequenced by Illumina HiSeq2000. Sequencing reads in fastq files were adaptor trimmed using a Perl script that implemented the procedure described in [43]. Next, ribosomal RNA sequences were filtered out by aligning them against a Bowtie2 index of the SBW25 rRNAs. The remaining reads were then aligned to the SBW25 genome to produce SAM files, which were used to calculate the centre-weighted coverage at each nucleotide position in the genome. For this, we used a Perl script to select alignments of between 23 and 41 nucleotides in length and counted for nucleotide positions after trimming 11 nucleotide positions from either end of the alignment. This was done separately for reads aligning to the forward and reverse genome strands and the centre-weighted coverage was stored in separate files for each strand. A separate Perl script was used to calculate RPKM values for each gene

based on strand specific centre-weighted coverages along the genome. The limma function plotMDS was then used to make PCA plots. The ribosome profiling data has been submitted to ArrayExpress, with accession number E-MTAB-5408.

Kinetic modelling

For each model, the chemical equations were translated into ordinary differential equations using mass action kinetics (S1 Table). Thermodynamic constraints were considered to ensure consistency between reaction rates via different routes, thereby reducing the number of free kinetic parameters. Kinetic forward rate constants were set to $10^9 \text{ M}^{-1}\text{s}^{-1}$ (diffusion limited) and equilibrium dissociation constants, K_d , were based on previous estimates—set initially to $1 \mu\text{M}$ and then optimized to fit with experimental data (see below). We used the ODE solver Vern7 from the Julia Differential Equations library to solve the chemical kinetics equations, which is suitable for high accuracy, non-stiff systems. Initial concentrations for cdG, RimK, RimA, and RimB were set to $1 \mu\text{M}$ unless specified otherwise, for instance when mimicking the conditions of a specific experiment as in S2 Fig. where [cdG] was $25 \mu\text{M}$. Solution of the ODE allowed us to determine steady state values for all RimK species for each model. These steady state concentrations were used to calculate the enzymatic modification of RpsF. K_m and k_{cat} values for each species of RimK and K_d values between Rim proteins were optimized to fit the model simulations to available experimental data, S2 Fig., using the Julia BlackBoxOptim library. Contributions of each RimK species to the kinetics with multiple species present were determined via optimization using all available data set simultaneously using Michaelis-Menton equations for the enzymatic reactions. Glutamation of the population was computed using a stochastic simulation that consisted of the addition of glutamate unit, the removal of a unit, or doing nothing. These probabilities are dependent on the concentration of the various RimK species and RimB. Average behaviour was computed from 1,000,000 independent stochastic simulations. All code was written in the free and open source scientific programming language Julia.

Supporting information

S1 Fig. (A) PCR of the *rim* operon from cDNA. The indicated band shows the position of the 2.2Kbp PCR product resulting from the amplification of the *rimABK* operon. **(B) Determining the transcription start site of the *rimABK* operon.** A cartoon representation of the *rimABK* operon and upstream region. Transcription initiation begins at one of the three nucleotides highlighted in red. The 5' RACE methodology does not allow discrimination between these nucleotides. **(C) *rimA* mRNA relative abundance does not substantially differ from that of *rimK*.** mRNA abundance (qRT PCR data) relative to cells grown overnight in LB and transferred to LB at 28°C and RS at 8°C for 45 minutes prior to sampling. RS—carbon free 'Rooting Solution' [19]. Data are presented +/- the standard error of three replicates. The experiment was repeated three times independently and a representative is shown. (TIF)

S2 Fig. ATPase assays suggest different activation states for RimK. This plot shows the experimental data from Fig 2E as points and the curves are computed from kinetic models based on RimA and cdG binding to RimK (S1 Table). Under the assumption that RimK can exist in two states, RimK and RimK*, with different activities and that RimK* achieved either by binding cdG or RimA, we simultaneously optimised all the parameters in the system (percentage of RimK*, k_{cat}^* and K_m^*). This plot shows that a simple two state model is consistent with the data. However, under this hypothesis and with [RimK] = $1 \mu\text{M}$, [RimA] = $1 \mu\text{M}$,

[cdG] = 25 μ M, the best fit to the ATPase data is achieved for an equilibrium dissociation constant (K_d) of 83.2 nM between RimK and RimA and 15.1 μ M between RimK and cdG. This is at odds with independent measurements that estimate K_d between RimK and cdG to be about 1 μ M [19]. This suggests that the simple two state system is unlikely and that RimK can exist in at least four different activation states (RimK, RimK.RimA, RimK.cdG and RimK.cdG.RimA, S1 Table). This model of RimK ATPase activity results in an insignificantly small better fit to the ATPase activity data but with a K_d between RimK and cdG of 1 μ M and a K_d between RimK and RimA of 0.2 μ M.

(TIFF)

S3 Fig. The $\Delta rimBK$ $rpsF_{4glu}$ mutant shows a loss of UV fluorescence and increased Congo Red binding on iron replete media. (A) Relative fluorescence (arbitrary units) at A_{460} of SBW25 mutant strains. WT SBW25 is shown in gold, $\Delta rimBK$ in blue and $\Delta rimBK$ $rpsF_{4glu}$ in orange. (B) Colony morphology resulting from 72-hour growth of 5 μ L spots of the indicated strains, on M9-pyruvate plates containing 0.004% Congo Red dye and 100 μ M $FeCl_2$.

(TIF)

S4 Fig. SBW25 $rimBK/rpsF$ mutations show distinct phenotypic changes. (A) Glutamation of RpsF at the C-terminus influences swarming motility. Overnight growth on swarm diameter plates containing 0.3% w/v agar and 0.05% Congo Red dye. (B) Colony morphology resulting from overnight growth of 5 μ L spots of the indicated strains, on KB agar plates containing 0.004% Congo Red dye. The presence of four C-terminal glutamates on RpsF results in smaller colonies and increased dye binding. (C) Growth curves in KB medium and (D) in M9-pyruvate medium. In both charts, WT SBW25 is shown in gold, $\Delta rimBK$ in blue, $\Delta rimBK$ $rpsF_{4glu}$ in orange and $\Delta rimBK$ $rpsF_{10glu}$ in green. The black line shows the absorbance of the uninoculated media.

(TIF)

S5 Fig. RpsF is incorporated into the ribosome in unmodified and highly glutamated states. Anti-RpsF immunoblot of ribosomes from different genetic backgrounds. Lane 1, molecular weight marker track (markers not resolved at this resolution). Lane 2, Purified hexa-histidine RpsF control. Cells were grown in either Lysogenic Broth media (denoted LB) at 28°C or Rooting Solution (denoted RS; [19]) at 4°C. WT, ΔBK , 4E and 10E denote ribosomes purified from wild-type, $\Delta rimBK$, $\Delta rimBK$ $rpsF_{4glu}$ and $\Delta rimBK$ $rpsF_{10glu}$ respectively.

(TIF)

S6 Fig. Distribution of all proteins quantified in Proteome Discoverer software (see iTRAQ method section) upon transition to cold, nutrient limiting conditions. Boxplots showing \log_2 -fold change ratios for protein abundance after: [45 minutes incubation in carbon-free rooting solution at 8°C]/[45 minutes incubation in LB medium at 28°C], for $\Delta rimK$ (mut) and WT SBW25 (wt).

(TIF)

S7 Fig. Scatterplots representing the pairwise comparisons of \log_2 ratios between the $\Delta rimBK$ $rpsF_{10glu}$ and $\Delta rimBK$ translomes. (A-C) Highlighted regions containing significantly ($>1.0 \log_2$) affected class 1, 2 and 3 genes respectively. (D) Genes significantly ($>1.0 \log_2$) affected by $rpsF$ glutamation but not significantly affected by $rimBK$ deletion. Highlighted genes are listed in S4 Table and colour-coded according to their COG classifications: yellow = metabolism; green = cellular processes and signalling; blue = information storage and processing; dark grey = poorly characterised.

(TIF)

S8 Fig. cdG binding to RimA in the presence of RimB could lead to cdG having a dual role in RimK regulation. Our experimental data show that both cdG and RimA increase the ATPase and glutamate activity of RimK in the absence of RimB. A model of RimA and cdG binding to RimK, leading to a state of higher activity, is consistent with this data (S2 Fig). In the presence of RimB, however, RimA becomes catalytically active, binding to and modifying cdG. Given the experimental data, a reasonable hypothesis is that this RimA activity promotes, either directly or indirectly, the dissociation from RimK. Here we model the effect of stimulating the RimK.RimA complex by cdG binding to RimK ($K_d = 1 \mu\text{M}$) and its inhibition by binding cdG to RimA ($K_d = 5 \mu\text{M}$) for different assumptions of different complex arrangements for RimK.RimA.

(TIFF)

S1 Table. Kinetic models for RimK ATPase activity.

(DOCX)

S2 Table. Effect of *rimK* deletion on relative protein abundance in different media conditions. Data are shown for all proteins differentially regulated in soluble cell lysates of SBW25 WT compared to $\Delta rimK$ after 45 minutes exposure to carbon free Rooting Solution at 8°C, or LB medium at 28°C. This list represents the proteins shown as coloured spots in Fig 8.

(XLSX)

S3 Table. Riboseq data for SBW25 $\Delta rimBK$. Genes whose translational activity is greater than \log_2 -fold up- or downregulated in SBW25 $\Delta rimBK$ compared to WT SBW25.

(XLSX)

S4 Table. Riboseq data for SBW25 $\Delta rimBK$ *rpsF*_{4glu/10glu}. Genes whose translational activity is greater than \log_2 -fold up- or downregulated in SBW25 $\Delta rimBK$ *rpsF*_{4glu/10glu} compared to $\Delta rimBK$.

(XLSX)

S5 Table. Class II and Class III RimK affected genes.

(XLSX)

S6 Table. Strains and plasmids used in this study.

(DOCX)

S7 Table. Primers used in this study.

(DOCX)

Acknowledgments

The authors would like to thank Carlo de Oliveira Martins for help and advice with the proteomic analysis.

Author Contributions

Conceptualization: Lucia Grenga, Richard Howard Little, Richard James Morris, Jacob George Malone.

Data curation: Govind Chandra, Gerhard Saalbach.

Formal analysis: Lucia Grenga, Richard Howard Little, Govind Chandra, Gerhard Saalbach, Richard James Morris, Jacob George Malone.

Funding acquisition: Richard James Morris, Jacob George Malone.

Investigation: Lucia Grenga, Richard Howard Little, Stuart Daniel Woodcock, Gerhard Saalbach, Richard James Morris.

Methodology: Lucia Grenga, Richard Howard Little, Govind Chandra, Gerhard Saalbach, Richard James Morris, Jacob George Malone.

Project administration: Jacob George Malone.

Resources: Gerhard Saalbach.

Software: Lucia Grenga, Govind Chandra, Richard James Morris.

Supervision: Jacob George Malone.

Validation: Govind Chandra, Gerhard Saalbach, Richard James Morris.

Visualization: Richard James Morris.

Writing – original draft: Richard Howard Little, Richard James Morris, Jacob George Malone.

Writing – review & editing: Lucia Grenga, Richard Howard Little, Govind Chandra, Gerhard Saalbach, Richard James Morris, Jacob George Malone.

References

1. Zhalnina K, Louie KB, Hao Z, Mansoori N, da Rocha UN, Shi S, et al. Dynamic root exudate chemistry and microbial substrate preferences drive patterns in rhizosphere microbial community assembly. *Nat Microbiol.* 2018; 3(4):470–80. Epub 2018/03/21. <https://doi.org/10.1038/s41564-018-0129-3> PMID: 29556109.
2. Lundberg DS, Lebeis SL, Paredes SH, Yourstone S, Gehring J, Malfatti S, et al. Defining the core *Arabidopsis thaliana* root microbiome. *Nature.* 2012; 488(7409):86–90. <https://doi.org/10.1038/nature11237> PMID: 22859206; PubMed Central PMCID: PMC4074413.
3. Mauchline TH, Malone JG. Life in earth—the root microbiome to the rescue? *Curr Opin Microbiol.* 2017; 37:23–8. <https://doi.org/10.1016/j.mib.2017.03.005> PMID: 28437662.
4. Alsohim AS, Taylor TB, Barrett GA, Gallie J, Zhang XX, Altamirano-Junqueira AE, et al. The biosurfactant viscosin produced by *Pseudomonas fluorescens* SBW25 aids spreading motility and plant growth promotion. *Environmental microbiology.* 2014; 16(7):2267–81. <https://doi.org/10.1111/1462-2920.12469> PMID: 24684210.
5. Chin-A-Woeng TFC, de Priester W, van der Bij AJ, Lugtenberg BJJ. Description of the Colonization of a Gnotobiotic Tomato Rhizosphere by *Pseudomonas fluorescens* Biocontrol Strain WCS365, Using Scanning Electron Microscopy. *Molecular Plant-Microbe Interactions.* 1997; 10(1):79–86. <https://doi.org/10.1094/mpmi.1997.10.1.79>
6. Campilongo R, Fung RKY, Little RH, Grenga L, Trampari E, Pepe S, et al. One ligand, two regulators and three binding sites: How KDPG controls primary carbon metabolism in *Pseudomonas*. *PLoS Genet.* 2017; 13(6):e1006839. <https://doi.org/10.1371/journal.pgen.1006839> PMID: 28658302; PubMed Central PMCID: PMC5489143.
7. Grenga L, Chandra G, Saalbach G, Galmozzi CV, Kramer G, Malone JG. Analysing the complex regulatory landscape of Hfq—an integrative, multi-omics approach. *Front Microbiol.* 2017; (8):1784.
8. Martinez-Granero F, Navazo A, Barahona E, Redondo-Nieto M, Gonzalez de Heredia E, Baena I, et al. Identification of flgZ as a flagellar gene encoding a PilZ domain protein that regulates swimming motility and biofilm formation in *Pseudomonas*. *PLoS one.* 2014; 9(2):e87608. <https://doi.org/10.1371/journal.pone.0087608> PMID: 24504373; PubMed Central PMCID: PMC3913639.
9. Jenal U, Reinders A, Lori C. Cyclic di-GMP: second messenger extraordinaire. *Nat Rev Microbiol.* 2017; 15(5):271–84. <https://doi.org/10.1038/nrmicro.2016.190> PMID: 28163311.
10. Barahona E, Navazo A, Martinez-Granero F, Zea-Bonilla T, Perez-Jimenez RM, Martin M, et al. *Pseudomonas fluorescens* F113 Mutant with Enhanced Competitive Colonization Ability and Improved Biocontrol Activity against Fungal Root Pathogens. *Appl Environ Microbiol.* 2011; 77(15):5412–9. Epub 2011/06/21. AEM.00320-11 [pii] <https://doi.org/10.1128/AEM.00320-11> PMID: 21685161; PubMed Central PMCID: PMC3147442.

11. Little RH, Woodcock SD, Campilongo R, Fung RKY, Heal R, Humphries L, et al. Differential Regulation of Genes for Cyclic-di-GMP Metabolism Orchestrates Adaptive Changes During Rhizosphere Colonization by *Pseudomonas fluorescens*. *Frontiers in Microbiology*. 2019; 10. ARTN 108910.3389/fmicb.2019.01089. WOS:000468022400001.
12. O'Neal L, Akhter S, Alexandre G. A PilZ-Containing Chemotaxis Receptor Mediates Oxygen and Wheat Root Sensing in *Azospirillum brasilense*. *Front Microbiol*. 2019; 10:312. Epub 2019/03/19. <https://doi.org/10.3389/fmicb.2019.00312> PMID: 30881352; PubMed Central PMCID: PMC6406031.
13. Ramos-Gonzalez MI, Travieso ML, Soriano MI, Matilla MA, Huertas-Rosales O, Barrientos-Moreno L, et al. Genetic Dissection of the Regulatory Network Associated with High c-di-GMP Levels in *Pseudomonas putida* KT2440. *Front Microbiol*. 2016; 7:1093. Epub 2016/08/05. <https://doi.org/10.3389/fmicb.2016.01093> PMID: 27489550; PubMed Central PMCID: PMC4951495.
14. Grenga L, Little RH, Malone JG. Quick Change—post-transcriptional regulation in *Pseudomonas*. *FEMS Microbiol Lett*. 2017. <https://doi.org/10.1093/femsle/fnx125> PMID: 28605536.
15. Valentini M, Filloux A. Biofilms and Cyclic di-GMP (c-di-GMP) Signaling: Lessons from *Pseudomonas aeruginosa* and Other Bacteria. *J Biol Chem*. 2016; 291(24):12547–55. Epub 2016/04/30. <https://doi.org/10.1074/jbc.R115.711507> PMID: 27129226; PubMed Central PMCID: PMC4933438.
16. Silby MW, Cerdano-Tarraga AM, Vernikos GS, Giddens SR, Jackson RW, Preston GM, et al. Genomic and genetic analyses of diversity and plant interactions of *Pseudomonas fluorescens*. *Genome Biol*. 2009; 10(5):R51. <https://doi.org/10.1186/gb-2009-10-5-r51> PMID: 19432983.
17. Moscoso JA, Jaeger T, Valentini M, Hui K, Jenal U, Filloux A. The diguanylate cyclase SadC is a central player in Gac/Rsm-mediated biofilm formation in *Pseudomonas aeruginosa*. *Journal of bacteriology*. 2014; 196(23):4081–8. <https://doi.org/10.1128/JB.01850-14> PMID: 25225264; PubMed Central PMCID: PMC4248864.
18. Moscoso JA, Mikkelsen H, Heeb S, Williams P, Filloux A. The *Pseudomonas aeruginosa* sensor RetS switches type III and type VI secretion via c-di-GMP signalling. *Environmental microbiology*. 2011; 13(12):3128–38. <https://doi.org/10.1111/j.1462-2920.2011.02595.x> PMID: 21955777.
19. Little RH, Grenga L, Saalbach G, Howat AM, Pfeilmeier S, Trampari E, et al. Adaptive Remodeling of the Bacterial Proteome by Specific Ribosomal Modification Regulates *Pseudomonas* Infection and Niche Colonisation. *PLoS Genet*. 2016; 12(2):e1005837. <https://doi.org/10.1371/journal.pgen.1005837> PMID: 26845436.
20. Irie Y, Starkey M, Edwards AN, Wozniak DJ, Romeo T, Parsek MR. *Pseudomonas aeruginosa* biofilm matrix polysaccharide Psl is regulated transcriptionally by RpoS and post-transcriptionally by RsmA. *Molecular microbiology*. 2010; 78(1):158–72. Epub 2010/08/26. <https://doi.org/10.1111/j.1365-2958.2010.07320.x> PMID: 20735777; PubMed Central PMCID: PMC2984543.
21. Brencic A, Lory S. Determination of the regulon and identification of novel mRNA targets of *Pseudomonas aeruginosa* RsmA. *Molecular microbiology*. 2009; 72(3):612–32. Epub 2009/05/12. MM16670 [pii] <https://doi.org/10.1111/j.1365-2958.2009.06670.x> PMID: 19426209.
22. Kino K, Arai T, Arimura Y. Poly-alpha-glutamic acid synthesis using a novel catalytic activity of RimK from *Escherichia coli* K-12. *Appl Environ Microbiol*. 2011; 77(6):2019–25. Epub 2011/02/01. <https://doi.org/10.1128/AEM.02043-10> PMID: 21278279; PubMed Central PMCID: PMC3067337.
23. Kaczanowska M, Ryden-Aulin M. Ribosome biogenesis and the translation process in *Escherichia coli*. *Microbiol Mol Biol Rev*. 2007; 71(3):477–94. Epub 2007/09/07. <https://doi.org/10.1128/MMBR.00013-07> PMID: 17804668; PubMed Central PMCID: PMC2168646.
24. Shen J, Meldrum A, Poole K. FpvA receptor involvement in pyoverdine biosynthesis in *Pseudomonas aeruginosa*. *Journal of bacteriology*. 2002; 184(12):3268–75. Epub 2002/05/25. <https://doi.org/10.1128/jb.184.12.3268-3275.2002> PMID: 12029043; PubMed Central PMCID: PMC135083.
25. Nait Chabane Y, Marti S, Rihouey C, Alexandre S, Hardouin J, Lesouhaitier O, et al. Characterisation of pellicles formed by *Acinetobacter baumannii* at the air-liquid interface. *PloS one*. 2014; 9(10):e111660. Epub 2014/11/02. <https://doi.org/10.1371/journal.pone.0111660> PMID: 25360550; PubMed Central PMCID: PMC4216135.
26. Poole P, Ramachandran V, Terpolilli J. Rhizobia: from saprophytes to endosymbionts. *Nat Rev Microbiol*. 2018; 16(5):291–303. Epub 2018/01/31. <https://doi.org/10.1038/nrmicro.2017.171> PMID: 29379215.
27. Schulz S, Eckweiler D, Bielecka A, Nicolai T, Franke R, Dotsch A, et al. Elucidation of sigma factor-associated networks in *Pseudomonas aeruginosa* reveals a modular architecture with limited and function-specific crosstalk. *PLoS Pathog*. 2015; 11(3):e1004744. Epub 2015/03/18. <https://doi.org/10.1371/journal.ppat.1004744> PMID: 25780925; PubMed Central PMCID: PMC4362757.
28. Lindenberg S, Klauck G, Pesavento C, Klauck E, Hengge R. The EAL domain protein YciR acts as a trigger enzyme in a c-di-GMP signalling cascade in *E. coli* biofilm control. *The EMBO journal*. 2013; 32

- (14):2001–14. Epub 2013/05/28. <https://doi.org/10.1038/emboj.2013.120> PMID: 23708798; PubMed Central PMCID: PMC3715855.
29. Loveland AB, Korostelev AA. Structural dynamics of protein S1 on the 70S ribosome visualized by ensemble cryo-EM. *Methods*. 2018; 137:55–66. Epub 2017/12/17. <https://doi.org/10.1016/j.ymeth.2017.12.004> PMID: 29247757; PubMed Central PMCID: PMC5866760.
 30. Duval M, Korepanov A, Fuchsbauer O, Fechter P, Haller A, Fabbretti A, et al. Escherichia coli ribosomal protein S1 unfolds structured mRNAs onto the ribosome for active translation initiation. *PLoS Biol*. 2013; 11(12):e1001731. Epub 2013/12/18. <https://doi.org/10.1371/journal.pbio.1001731> PMID: 24339747; PubMed Central PMCID: PMC3858243.
 31. Sukhodolets MV, Garges S. Interaction of Escherichia coli RNA polymerase with the ribosomal protein S1 and the Sm-like ATPase Hfq. *Biochemistry*. 2003; 42(26):8022–34. Epub 2003/07/02. <https://doi.org/10.1021/bi020638i> PMID: 12834354.
 32. Kambara TK, Ramsey KM, Dove SL. Pervasive Targeting of Nascent Transcripts by Hfq. *Cell Rep*. 2018; 23(5):1543–52. Epub 2018/05/03. <https://doi.org/10.1016/j.celrep.2018.03.134> PMID: 29719264; PubMed Central PMCID: PMC5990048.
 33. Carmichael GG, Weber K, Niveleau A, Wahba AJ. The host factor required for RNA phage Qbeta RNA replication in vitro. Intracellular location, quantitation, and purification by polyadenylate-cellulose chromatography. *J Biol Chem*. 1975; 250(10):3607–612. Epub 1975/05/25. PMID: 805130.
 34. Wahba AJ, Miller MJ, Niveleau A, Landers TA, Carmichael GG, Weber K, et al. Subunit I of G beta replicase and 30 S ribosomal protein S1 of Escherichia coli. Evidence for the identity of the two proteins. *J Biol Chem*. 1974; 249(10):3314–6. Epub 1974/05/25. PMID: 4208476.
 35. Inouye H, Pollack Y, Petre J. Physical and functional homology between ribosomal protein S1 and interference factor i. *Eur J Biochem*. 1974; 45(1):109–17. Epub 1974/06/01. <https://doi.org/10.1111/j.1432-1033.1974.tb03535.x> PMID: 4213953.
 36. Kang WK, Icho T, Isono S, Kitakawa M, Isono K. Characterization of the gene rimK responsible for the addition of glutamic acid residues to the C-terminus of ribosomal protein S6 in Escherichia coli K12. *Molecular & general genetics: MGG*. 1989; 217(2–3):281–8. Epub 1989/06/01. <https://doi.org/10.1007/BF02464894> PMID: 2570347.
 37. Miller JH. *Experiments in molecular genetics*. Cold Spring Harbor Laboratory, Cold Spring Harbor, New York. 1972:352–5.
 38. Little R, Salinas P, Slavny P, Clarke TA, Dixon R. Substitutions in the redox-sensing PAS domain of the NifL regulatory protein define an inter-subunit pathway for redox signal transmission. *Molecular microbiology*. 2011; 82(1):222–35. Epub 2011/08/23. <https://doi.org/10.1111/j.1365-2958.2011.07812.x> PMID: 21854469.
 39. Scott TA, Heine D, Qin Z, Wilkinson B. An L-threonine transaldolase is required for L-threo-beta-hydroxy-alpha-amino acid assembly during obafuorin biosynthesis. *Nat Commun*. 2017; 8. ARTN 1593510.1038/ncomms15935. WOS:000404029700001.
 40. King EO, Ward MK, Raney DE. Two simple media for the demonstration of pyocyanin and fluorescein. *The Journal of laboratory and clinical medicine*. 1954; 44(2):301–7. Epub 1954/08/01. PMID: 13184240.
 41. Perez-Riverol Y, Csordas A, Bai J, Bernal-Llinares M, Hewapathirana S, Kundu DJ, et al. The PRIDE database and related tools and resources in 2019: improving support for quantification data. *Nucleic Acids Res*. 2019; 47(D1):D442–D50. Epub 2018/11/06. <https://doi.org/10.1093/nar/gky1106> PMID: 30395289; PubMed Central PMCID: PMC6323896.
 42. Oh E BA, Sandikci A, Huber D, Chaba R, Gloge F, Nichols RJ, Typas A, Gross CA, Kramer G, Weissman JS, Bukau B. Selective ribosome profiling reveals the cotranslational chaperone action of trigger factor in vivo. *Cell*. 2011; 147(6):1295–308. <https://doi.org/10.1016/j.cell.2011.10.044> PMID: 22153074
 43. Becker AH, Oh E, Weissman JS, Kramer G, Bukau B. Selective ribosome profiling as a tool for studying the interaction of chaperones and targeting factors with nascent polypeptide chains and ribosomes. *Nat Protoc*. 2013; 8(11):2212–39. <https://doi.org/10.1038/nprot.2013.133> WOS:000326164100010. PMID: 24136347